Initial Orbit Determination (IOD) of Resident Space Objects (RSO) Using Space-based Single- and Multi-site Optical Observations

Marianna Veltri

A Thesis Submitted to the Faculty of Graduate Studies
In Partial Fulfillment of the Requirements
for the Degree of Master of Science

Earth and Space Science

York University
Toronto, Ontario

July 2026

©Marianna Veltri, 2026

Abstract

Millions of Resident Space Objects (RSOs) orbit Earth, most of which are not tracked. Space Situational Awareness (SSA) research provides knowledge of RSOs and their orbits to maintain a safe space environment and mitigate the ongoing threat of RSO congestion and collisions. A significant component of SSA is calculating initial orbit determinations (IODs) of RSOs using single-site optical observations. However, these observations cannot always provide accurate IODs or direct range measurements, so this research proposes using multi-site optical observations. Noted for its robustness, Gooding's IOD method is used to compare IOD accuracy from single- and multi-site observation for RSOs in different orbits. Results show that one multi-site scenario produced IOD with a decrease in the overall magnitude of error by approximately 88% for position, 91% for velocity, and 97% for range values for RSOs in low Earth orbit. Ultimately, multi-site observations can significantly improve IOD accuracy for SSA endeavours.

Acknowledgments

I am extremely blessed and grateful for all the support that I have received throughout my graduate studies. A sincere thank you to my supervisor, Regina Lee, whose constructive guidance and expertise encouraged me to improve throughout the course of my studies. Thank you to my peers and lab members for your collaboration, supportive feedback, and willingness to share your knowledge with me. To my friends, thank you for all your encouragement and advice you have given me throughout this journey. I am especially grateful to my family for their unwavering support and patience. Their constant faith in me has been a foundation throughout all my academic pursuits. Finally, I would like to thank my partner for his never ending encouragement, understanding and support. His patience and reassurance has been a constant source of strength which kept me focused and motivated, especially during challenging moments of this work.

Table of Contents

Page

Abstract . . . . . **ii**

Acknowledgments . . . . . **iii**

Table of Contents . . . . . **iv**

List of Tables . . . . . **vi**

List of Figures . . . . . **vii**

List of Acronyms . . . . . **viii**

Chapter 1: Introduction **1**

1.1 Motivation and Problem Statement 1

1.2 Research Objectives 3

1.3 Methodology 4

1.4 Thesis Overview 6

Chapter 2: Background **8**

2.1 Resident Space Object (RSO) Population 8

2.1.1 Resident Space Objects in Different Orbits 8

2.1.2 Two-line Element Set 10

2.2 Space Situational Awareness (SSA) 11

2.2.1 Demand for SSA due to RSO Population 11

2.2.2 RSO Observations Using Star-trackers 12

2.3 Initial Orbit Determination (IOD) 13

2.3.1 IOD Description 14

2.3.2 Initial Orbit Determination vs Orbit Determination vs Precise Orbit Determination 16

2.3.3 Space-Based and Ground-Based Optical Observations of RSOs 17

2.3.4 Position and Velocity Vectors to Classical Orbital Elements (COE) 18

2.3.5 Single-Site Observations of RSOs 25

2.3.6 Multi-site Observations of RSOs 26

2.3.7 Obtaining RSO Range and Position Vectors from Star-trackers 27

2.3.8 Gooding's Method 31

2.3.9 Related Work 33

Chapter 3: Simulation Processes 37
3.1 Scenario Set-up and Data Collection 37
3.2 Ansys System Tool Kit (STK) 38
3.2.1 Ansys System Tool Kit Single-site Scenarios 40
3.2.2 Ansys System Tool Kit Multi-site Scenarios 43
3.3 Gooding's Algorithm Using Single- and Multi-site Data 50
3.3.1 Access Reports 51
3.3.2 LOS and Range Calculations Using Simulated Data 54
3.3.3 Final Input Values for Gooding's Algorithm 56

Chapter 4: Results 58
4.1 LEO Results 58
4.1.1 LEO Results Analysis 62
4.2 MEO Results 64
4.2.1 MEO Results Analysis 67
4.3 GEO Results 68
4.3.1 GEO Results Analysis 71
4.4 Overall Result Analysis 73

Chapter 5: Conclusion 75
5.1 Overview of Thesis 75
5.2 Contributions 76
5.3 Future Work 78

References 81

List of Tables

1 Various types of orbital debris 9
2 IOD methods 16
3 Eccentricity ranges 22
4 Gooding's algorithm inputs and outputs 33
5 Access report single-site scenario 52
6 Access report SL 3-site 52
7 Access report SL 2-site 53
8 Access report DL 3-site 53
9 Access report DL 2-site 54
10 Gooding's algorithm inputs example 57
11 Gooding's algorithm output example 57
12 LEO standard deviation results 58
13 LEO root mean square error results 59
14 MEO standard deviation results 64
15 MEO root mean square error results 65
16 GEO standard deviation results 68
17 GEO root mean square error results 69

List of Figures

1 RSO abundance 2
2 Research Overview 6
3 TLE 11
4 Observational arcs 14
5 Geocentric equatorial coordinate frame 19
6 Inclination 23
7 Right ascension of ascending node 24
8 Argument of perigee 24
9 Star-tracker images 28
10 Parallax 28
11 RSO position vector 31
12 Scenario Orientations 40
13 STK Single-site host 42
14 STK Single-site RSOs 43
15 STK straight line multi-site hosts 46
16 STK diagonal line multi-site hosts 49
17 STK Multi-site RSOs 50
18 RMSE comparison between two scenarios for RSOs in LEO 61
19 Observation arc LEO 63
20 RMSE comparison between two scenarios for RSOs in MEO 66
21 RMSE comparison between two scenarios for RSOs in GEO 70

List of Acronyms

RSO Resident Space Object

SSA Space Situational Awareness

IOD Initial Orbit Determination

CASSIOPE Cascade SmallSat IOnospheric Polar Explorer

STK Ansys System Tool Kit

FOV Field of View

FAI Fast Auroral Imager

LEO Low Earth Orbit

MEO Medium Earth Orbit

GEO Geostationary Earth Orbit

TLE Two-Line Element

OD Orbit Determination

POD Precise Orbit Determination

ASAT Anti-satellite

COE Classical Orbital Elements

KE Kinetic Energy

PE Potential Energy

RAAN Right Ascension of the Ascending Node

LOS Line-of-Sight

AU Astronomical Units

ECI Earth-Centered Inertial

HEO Highly Elliptical Orbits

SL Straight Line Simulation

DL Diagonal Line Simulation

SIM Simultaneous

RMSE Root Mean Square Error

Chapter 1: Introduction

1.1 Motivation and Problem Statement

More than one hundred million Resident Space Objects (RSOs) are in orbit around our planet including active satellites, crewed stations, rocket bodies and other space debris [1] [2]. Active satellites greatly contribute to society with aspects such as communication, scientific research, live broadcasts, banking, navigation, and more. Satellites are crucial for everyday life around the world and are essential for our ever-growing technological world. Currently, only about 45,000 of these RSOs are regularly tracked and cataloged by space surveillance networks, leaving millions of RSOs unaccounted for in these catalogs [1]. The RSO population will continue to grow due to future launches and fragmentations of existing RSOs. Fragmentations of RSOs can be caused by collisions of two or more objects, electronic explosions, design flaws, and interactions with Earth's atmosphere [1]. These events lead to an increase in the number of unaccounted for and unknown RSOs in different orbits around Earth. These unaccounted for RSOs can cause further collisions and issues with other objects, causing a domino effect. Human life on Earth relies heavily on satellites, so it is valuable to understand the orbital characteristics of all RSOs in orbit around our planet to ensure a safe space environment and further technological advancements.

Space Situational Awareness (SSA) is a growing field of study that provides knowledge and characterization of RSOs and their orbits. SSA also involves understanding and predicting RSO locations in order to maintain a safe and sustainable space environment around Earth [3] [4]. Therefore, the growing population of RSOs is a major concern within modern SSA research. This congestion could lead to an unwanted increase in collisions, which pose great threats to active satellites, future launches, and crewed stations. The evolution of the number of objects in orbit around Earth throughout many years is seen in Figure 1 [1].

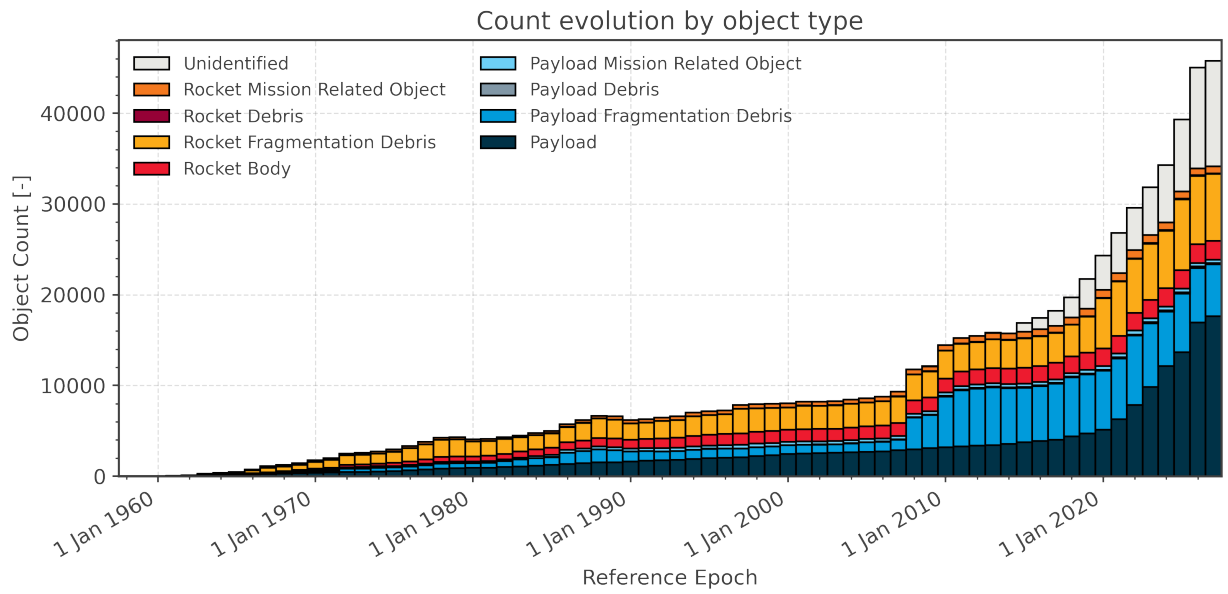

Figure 1: The count evolution for the total number of tracked RSOs that orbit Earth. The RSOs are grouped by object type, some which include fragmentation debris and unidentified objects. The area of these objects have an approximate upper-bound of 350,000 m^2. Image Credit: [1].

A large component of SSA is using Initial Orbit Determination (IOD) of RSOs to obtain an initial calculation of its orbital parameters. Angles-only observations for IOD are performed using optical imagers, where the azimuth and elevation of an object can be obtained from the images and used to calculate the RSOs position and velocity vectors [5]. These angles-only observations are obtained from either ground-based or space-based stations, each with their own advantages and disadvantages.

The current most widespread practice for obtaining IODs is using a single-site observations. However, using optical data from only one site does not yield accurate classical orbital parameters or range measurements [6]. With advancing IOD research, there are suggestions for using multi-site observations because they could provide additional data, improved IOD accuracy, and range measurements [6]. IODs are fundamental for SSA purposes because they provide classical orbital parameters of objects in orbit around earth. Knowing these parameters can aid in collision detection and prevention methods to help maintain indispensable satellites and crewed stations.

This challenging task is extremely important considering that the current way of obtaining IODs is not accurate and does not provide direct range measurements [6]. However, using multi-site observations could be the solution. Providing accurate IODs and range measurements of RSOs using multi-site observations is a clear next step for SSA. With improved accuracy of IODs due to multi-site observations, we can keep track of accurate orbital parameters of RSOs and use them to prevent catastrophic collisions.

1.2 Research Objectives

The overall aim of this research is to determine if multi-site observations will improve IOD accuracy for SSA purposes. For multi-site observations to be beneficial to SSA, they must contribute something that current single-site observations do not. Presently, IODs are most commonly obtained by using single-site observations with outputs that lack range measurements and accurate orbital information. To obtain range measurements of RSOs, observations must be done at various locations, hence the need for multi-site observations. These multi-site observations also allow for improved accuracy in calculating IODs; which is extremely critical for numerous SSA objectives. While using multiple observation sites is not a new concept, there is still a lot of missing information due to minimal research. In most of the literature, multi-site observations are part of future research plans, and any testing done on this topic is limited.

While most multi-site research found in the literature focuses on using two observers, this thesis tests the accuracy of IODs calculated from space-based observations done with a singular host, double hosts, and triple hosts. Additionally, while most literature focuses on RSOs in one orbit, this research takes it a step forward by observing RSOs in low, medium, and geostationary orbits; allowing for a broader idea of how multi-site observations improve IOD and range from objects in a variety of orbits. Furthermore, two different constellation formations for the multi-site observations are studied to see which geometry, if any, produce more accurate IODs. From these objectives, a full comparative analysis between all space-based single- and multi-site observational scenarios can be done, to see which is the finer option for obtaining more accurate IODs as a whole.

Many satellites have star-trackers on board solely for attitude determination, yet they can also be used for RSO detection and observations [7]. The idea of using star-trackers onboard active satellites for RSO observations has been studied and heavily supported within the literature [7][8][9][10]. Nevertheless, there is a gap in the research which involves testing the usability of these images for IOD purposes. This thesis demonstrates that star-tracker images can be used for IOD observations and calculations, and thus is only testing space-based observations.

The main objectives within this thesis which aim to benefit SSA research include:

1. Demonstrating how space-based star-tracker images can be used for IOD observations and calculations of RSOs

2. Evaluating whether space-based multi-site observations produce more accurate IODs than space-based single-site observations by comparing results from a singular host, double hosts, and triple hosts configurations

3. Determining if space-based multi-site observations can be used to obtain accurate IODs of objects in low, medium and geosynchronous orbits

4. To investigate whether host-satellite constellation geometry, specifically a straight line versus a diagonal line formation, has a discernible effect on IOD accuracy

1.3 Methodology

There are no publicly available multi-site observations, so a simulation software is used to create the data needed for this research. In order to obtain IODs and range measurements, ephemeris and TLE data is used to simulate the Cascade SmallSat IOnospheric Polar Explorer (CASSIOPE) satellite and the observed RSOs [11][12]. The CASSIOPE ephemeris data is used for the single-site host and is then used as a basis for the multiple other hosts created [11]. The various scenarios tested in this thesis are created using the Ansys Systems Tool Kit (STK) to validate the orientations and parameters for the multiple satellite systems [12]. Additionally, a sensor, consistent with the

specifications of the Fast Auroral Imager (FAI), is used to represent an onboard star-tracker [13]. A detailed description of the simulation process can be seen in Chapter 3.

Gooding's algorithm is chosen to calculate IOD of the RSOs because of its robustness and accuracy noted within the literature [14]. His algorithm provides the position vector, velocity vector, and range measurements of the observed RSOs [14]. From these results provided by his algorithm, and accuracy comparison between single- and multi-site observations can be studied.

The remainder of this thesis is dedicated to an in-depth comparison between the space-based single- and multi-site observations. The comparison will include advantages and disadvantages for both observation methods and look at RSOs in Low Earth Orbit (LEO), Medium Earth Orbit (MEO), and Geostationary Earth Orbit (GEO) orbits. From these comparisons, one can determine if it is logical to continue with single-site observations or if it is beneficial to push for multi-site observations for SSA purposes instead. A general overview of the research process can be seen in Figure 2.

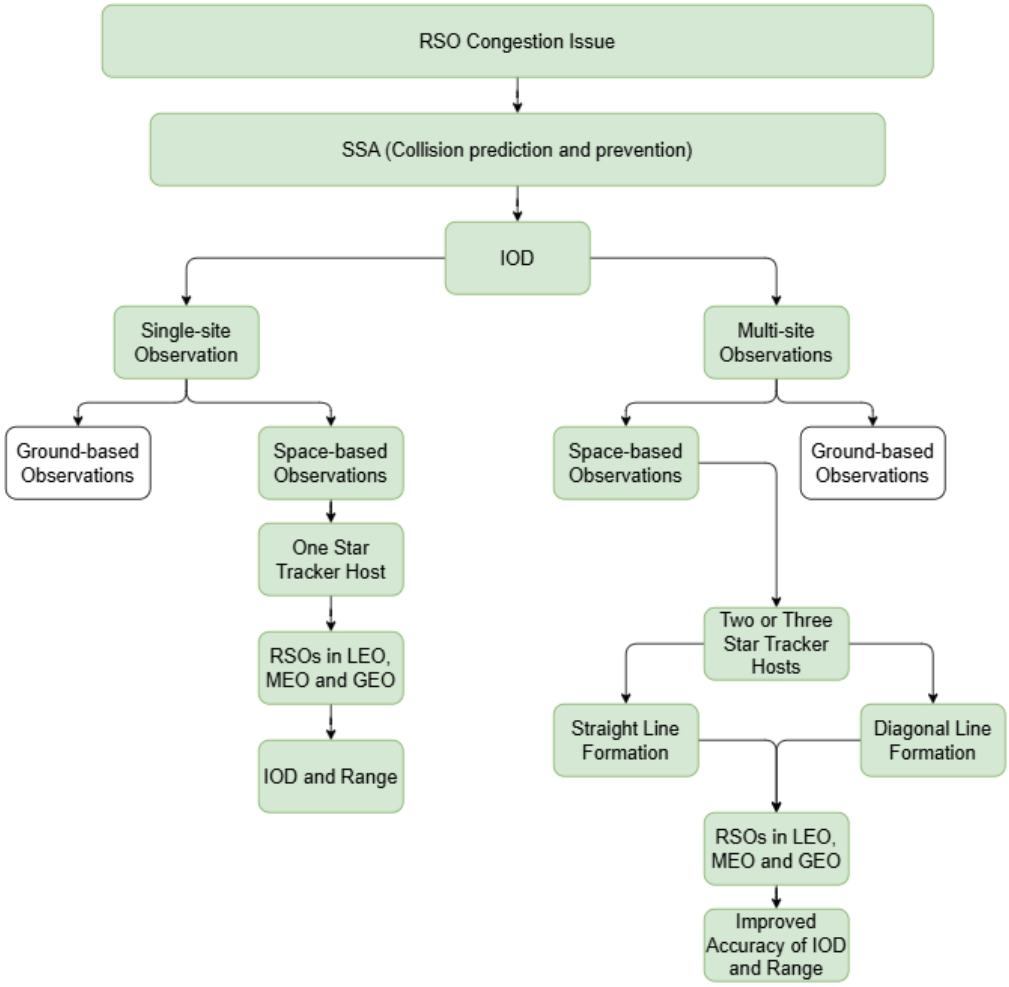

Figure 2: Overview of research process. The boxes in green are prominent research points within this thesis.

1.4 Thesis Overview

Chapter 2 discusses the necessary background information on the topics of this research such as RSO abundance, SSA research, and IOD practices. It provides the necessary information on the theoretical and mathematical techniques relevant to this research, and using star-trackers for IOD calculations. In Chapter 3, the scenario creations, data collection, and the chosen IOD method is described. It demonstrates how the simulation tool is used and provides the steps for generating the data. Chapter 4 provides the results from the single- and multi-site observations with an analysis of important discoveries and comparisons. It forms conclusions to the objectives relating single- and multi-site observations; determining if multi-site observations are suitable for observing RSOs

in different orbits, and creating a basis for formation flying IOD research. Lastly, Chapter 5 draws conclusions for the debate between single-site and multi-site IOD observations for SSA purposes, and discusses possible future research within this field.

Chapter 2: Background

Space Situational Awareness (SSA) is a fundamental aspect for the safety of space operations. The overcrowding of resident space objects (RSOs) in orbit around our planet is causing a growing demand for orbital information on these objects regarding collision prevention strategies. As a result, this demand has brought forth research methodologies which explore the orbital characteristics of RSOs. This research specifically focuses on Initial Orbit Determination (IOD) of RSOs. Modern research on IODs uses data from single-site observations, however, this research advances this process through multi-site observations. The leading focus of this research lies in improving the accuracy of current IOD methods to advance SSA objectives.

2.1 Resident Space Object (RSO) Population

The growing demand for RSO characterization illustrates the pressing issues of RSO overcrowding and collision probability within all orbits around Earth. Many active satellites can be found in Low Earth Orbit (LEO), Medium Earth Orbit (MEO), and Geostationary Orbit (GEO) along with other uncharacterized or unaccounted for RSOs. Since each of these orbits hosts valuable satellites, it raises great concern about the possibility of unpredictable collisions. In addition, characteristics of these RSOs and their orbits are necessary for future launches and other research pursuits. As a result, understanding RSOs in greater detail is crucial for SSA endeavors.

2.1.1 Resident Space Objects in Different Orbits

RSOs are objects which reside in various orbits around Earth such LEO, MEO, and GEO [1]. The abundance of RSOs spans the many orbital regimes and includes many diverse types of objects such as active satellites, inactive satellites, and different forms of debris including [1][15]:

Objects	Description
Rocket Bodies	Objects apart of launch related functionality
Rocket Mission Related	Space objects intentionally released after serving purpose for a rocket body
Fragmentation Debris	Objects unintentionally released from other objects due to fragmentation events
Payload Debris	Objects unintentionally released from payloads
Unidentified	Other uncategorized objects of unknown origin

Table 1: Various types of orbital debris [1].

With these objects, and many others, there are more than one hundred million RSOs in orbit around our planet today [1]. From the time of writing this thesis only around 45,000 of these objects are regularly tracked by Space Surveillance Networks and maintained in their corresponding catalogs [1]. This means most RSOs are not tracked or cataloged, causing a pressing concern for catastrophic collisions. Furthermore, fragmentation of RSOs causes an increase in the number of objects orbiting our planet [15]. Plenty of these fragments and their origins go unnoticed, as many are produced without our knowledge. That said, the ever-increasing RSO population with unknown orbital parameters is a pressing concern for Space Situational Awareness.

Many of the orbits around Earth are occupied with RSOs and space debris, some more than others. LEO, which is at an altitude of 2,000 km or less, is known to host the majority of RSOs with a cataloged population of around 26,000 [1]. This orbit hosts most of the active satellites and is home to a large majority of space debris, raising great concern about the possibility of collisions [2]. MEO, which is at an approximate altitude of around 2,000 km to 35,500 km, hosts around

1000 cataloged objects, many being communication and navigation satellites [1]. GEO, which is at an altitude of approximately 35,500 km to 36,000 km is home to around 900 cataloged objects that include weather and entertainment broadcasts [1]. For these three orbits and all others, there is around a total of 45,000 cataloged objects which is nowhere near the actual amount of RSOs that orbit our planet [1]. The lack of information on the millions of other RSOs, and risks of fragmentations, poses a great concern for catastrophic collisions with essential active satellites and even crewed stations.

2.1.2 Two-line Element Set

RSO identification and orbital parameters play vital roles in tracking important space objects and debris. In the field of SSA, this information is crucial for identifying and tracking RSOs. Two-line Element (TLE) sets are the main tool for this. TLE sets are a data format, encoding a list of parameters and orbital elements of RSOs used for various SSA purposes. The first line consists of information such as the catalog number, also known as NORAD ID, RSO name, and International Designator [16][17]. The second line includes more information on the orbit of the RSO such as inclination, eccentricity, mean anomaly, argument of perigee, and more [16][17]. These orbital values are necessary for locating and tracking known objects for a variety of reasons, such as collision prevention and scientific research. TLEs can also be used with the help of a propagator, such as SGP4, to propagate the position of the RSO. The TLE parameters and format are shown below in Figure 3 [18].

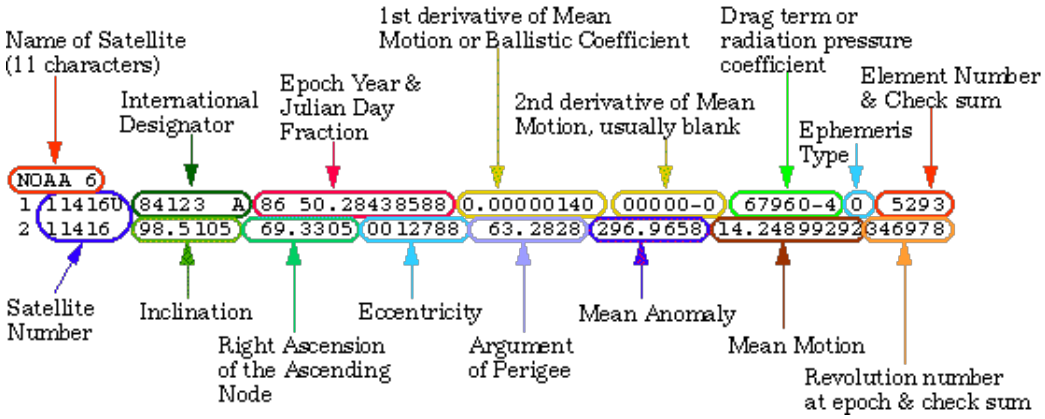

Figure 3: TLE orbital information breakdown [18].

2.2 Space Situational Awareness (SSA)

Space Situational Awareness focuses on maintaining a safe and sustainable environment in the orbits around Earth. Through modern research, there are many approaches for SSA research, all with the end goal of maintaining our space environment. RSO detection, identification, and orbit determination, are some main objectives of SSA and are continuously being worked on and improved as seen in the literature. Initial orbit determination is a very important path within modern research for SSA. This research will focus specifically on RSO orbital information for SSA purposes.

2.2.1 Demand for SSA due to RSO Population

Space Situational Awareness is a growing field of study that focuses on collecting and monitoring data on RSOs in orbit around Earth. Recently, there has been a steady increase in RSOs because of the increase in satellite launches [19]. In addition, fragmentations of existing RSOs are becoming more frequent due to collisions with other RSOs and categorized objects [1]. With that said, over one hundred million RSOs orbit our planet, most of them unaccounted for [1]. The considerable number of RSOs poses a great concern for the field of SSA due to the increased probability of unwanted collisions.

A large part of SSA is obtaining orbital information of RSOs for tracking and collision prevention purposes through Initial Orbit Determination (IOD). There are many different mathematical

methods for IOD, the most common being Gauss' and Laplace methods which involve angles only observations [5][20]. One process for obtaining these observations is using space-based star-trackers. Star-trackers are beneficial for SSA research because they provide a cheap and effective method for observing RSOs and will be discussed in more detail in Chapter 2.2.2 [19][21].

2.2.2 RSO Observations Using Star-trackers

The first step for IOD is detecting and collecting data on the RSOs. There is a push for SSA technological advancements due to the rapid growth in the RSO population. Many approaches for RSO detection involve using various imaging technologies for both ground- and space-based observations. A widely adopted form of RSO detection is ground-based and space-based optical imaging, which is discussed in Chapter 2.3.3. A wide variety of ground-based optical telescopes are available worldwide. However, a major downside is that weather and atmospheric conditions affect the quality of data collection. One way to combat this is by using optical imagers aboard a satellite such as star-trackers.

Star-trackers are a very common imaging instrument onboard many satellites and are typically used for attitude determination of the spacecraft [7]. The camera takes periodic images of the stars in its Field of View (FOV), then using a star catalog, an algorithm estimates the orientation of the satellite based on the star's locations in the images [7]. Star-trackers capture the light produced by the stars themselves, however, it can also capture reflected light from RSOs [7][9]. The minimum brightness a star-tracker can capture is highly dependent on the specific technology itself, along with exterior reasons. This means that the star-trackers signal-to-noise ratio can cause limitations on the amount of objects the imager can detect. Nonetheless, using the reflection from the RSO gives star-trackers a dual purpose for RSO detection and has been considered in detail for Space Situational Awareness [7][8][9][10][19][22]. The ongoing research on a star-trackers ability to detect and track RSOs via stratospheric balloon missions and space-based observers further supports validity for its use in other areas of study such as IOD [23][24][25][26]. Since star-trackers are confirmed to be a strong candidate for RSO detection, this thesis supports the idea of using their images to provide

the necessary numerical data needed for IOD processes [7][8][9][10][19][22][23][24][25][26][27].

A star-tracker's ability to observe RSOs is ideal because thousands of star-trackers are currently in orbit around Earth. A large amount of active satellites use star-trackers, so obtaining optical observations of RSOs from not just one satellite, but multiple at the same time, is possible [9]. One way to determine whether multiple star-trackers are observing the same RSO is by calculating and comparing the spacial positions of the RSO from the star-tracker images [9]. Then, IOD is calculated from each host observer separately. By doing so, the Classical Orbital Elements (COE) can be compared; if the orbital elements calculated by each host are similar, then it is safe to assume that these separate observations are of the same RSO [9]. Finally, the observational data from the multiple hosts can be combined and used for multi-site IOD calculations.

This thesis adds to the work done regarding dual-purpose star-trackers by demonstrating that star-tracker observations can also be used for IOD purposes. Furthermore, this research compares IOD results from single-site and multi-site observations done with star-trackers. Therefore, a star-tracker's ability to detect RSOs is revolutionary and is the main technology used for discussion of IOD throughout this thesis.

2.3 Initial Orbit Determination (IOD)

Initial orbit determination is a main focus within SSA research. IODs provide classical orbital parameters of RSOs within any orbit around Earth. Observations can be performed in space- or ground-based locations, both having advantages and drawbacks. IOD requires an RSO to be observed at least three separate instances in order to form an arc of the object's orbits, and to determine the RSO state vectors which require six independent quantities [5]. A widely adopted strategy for initial orbit determination is the use of single-site observations. However, this research proposes using multi-site space-based observations to strengthen the accuracy of IODs of RSOs.

2.3.1 IOD Description

IOD is a crucial part of SSA research since it supports the study and tracking of RSO orbital information. This initial step in orbit determination does not require any prior information and produces estimates of an RSO's classical orbital elements from position and velocity vectors. IOD is critical for obtaining and maintaining accurate orbital information [28].

Fundamentally, angles-only observations consist of line-of-sight unit vector data of a RSO from a space-based observer, which is obtained from optical images [5]. IOD calculations require an RSO to be observed at three instances to form an arc of its full orbit and to determine the RSO state vectors [5]. An example of the arc from three observations can be seen in Figure 4A. Having three angles-only observations gives the minimum number of variables needed (six) for input values to calculate the position and velocity vectors of the RSO [5]. However, a common issue could arise from these three observations; the too-short-arc problem. This problem arises when the three observations form an arc that is too short for proper IOD calculations, due to limited data that has a high degree of similarities [29]. An example of a too-short-arc can be seen in Figure 4B. The too-short-arc problem is a significant challenge for single-site optical observations when the data is sparse [29].

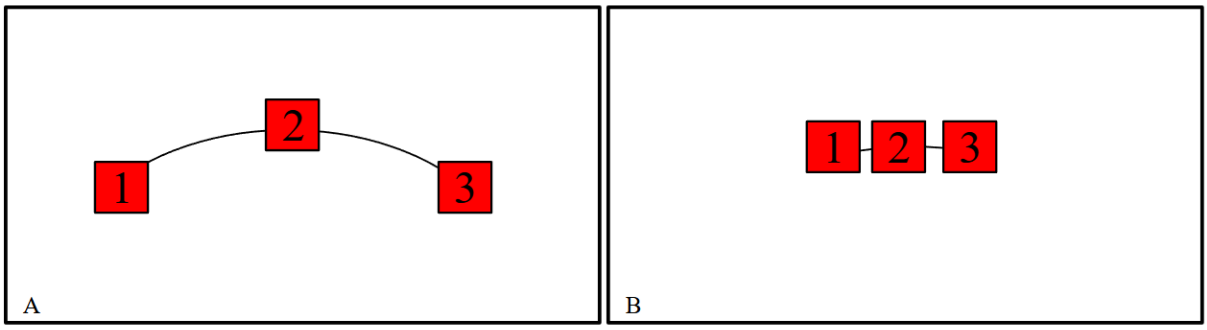

Figure 4: Example of observational arcs. The red boxes represents the RSO being observed at three instances. Image A represents an arc of the RSOs orbit which is formed from the three observations. Image B represents the too-short-arc problem.

IOD methods vary depending on the information available such as initial parameters, assump-

tions, limitations, data collection process, and more. Many methods for calculating angles-only IOD involve using Gauss' or Laplace's methods, both of which are used in modern research. These methods are commonly used for observations done via optical sensors, with major drawbacks such as the absence of direct range measurements and limitations in accuracy. The ideal choice of IOD methods depends heavily on a variety of specifications, which further pushes researchers to revamp existing methods or produce innovative solutions.

Initial orbit determinations via optical observations, encounter many challenges in achieving accurate results due to restrictive observational data collection processes and no prior data [30]. Improving the accuracy and precision of these calculations is a primary concern for SSA research due to the importance of tracking orbital parameters of RSOs. With this push for improved IOD accuracy, many IOD mathematical processes are created, adjusted, and tested. Some processes can even provide range measurements between the observer and RSO. That said, Table 2 provides basic information on a few classical IOD methods that are commonly found and used within the literature, and Chapter 2.3.9 dives into research done on these three IOD algorithm performances [5][14].

IOD Method	IOD Description
Laplace	Used to estimate the middle position and velocity vectors for natural celestial objects. Not accurate for artificial satellite objects.
Gauss	Is most accurate when used for interplanetary studies but is somewhat robust when used for artificial satellite objects under certain scenarios.
Gooding	A general solution to the angles-only problem which uses a higher-order Newton correction and solves Lamberts orbital boundary-value problem. There are no restriction on the three observing sites. It is more robust than Laplace's or Gauss' methods.

Table 2: Angles-only initial orbit determination methods [5][14].

2.3.2 Initial Orbit Determination vs Orbit Determination vs Precise Orbit Determination

Initial orbit determination, orbit determination, and precise orbit determination are all complex processes that are used to determine the orbit of a RSO. IOD is the initial step for approximating the orbit of an object and is used as a baseline for orbit determination (OD) and precise orbit determination (POD) [28][30]. Many researchers consider OD as an umbrella term for orbital research as a whole, while POD is considered the following step after IOD. Similarly in literature, many use OD and POD interchangeably. Due to this inconsistency, this thesis considers OD as an umbrella term for orbital research as a whole, and POD as the process following IOD.

IOD is calculated using limited observational data, usually containing noise, and does not take into consideration perturbations or other factors [30]. The main purpose of IOD is to determine the RSOs state vector and to form a baseline understanding of its orbit as described in Chapter 2.3.1. While the accuracy of this initial step depends on factors such as camera quality and parameters, it

is not considered in the calculations of IOD. In simple terms, IOD is the starting point for OD.

POD uses IOD as the foundation and iteratively refines the results. A common way to do this is to use the concept of least square estimation and to consider factors such as perturbations and camera parameters [20][30]. Certain POD models which help refine IOD via perturbations effects include solar radiation models, atmospheric drag models, and gravity field models [30]. Additionally, sensor measurements errors, camera parameters, and other technological uncertainties are also taken into account when calculating POD [20][30]. To do these refinements, more observations are taken in order to find information that might have been missed within the 3 initial observations used for IOD. While POD processes are not the focus of this thesis, there are many detailed processes that can be found within the literature [20][30].

With that said, IOD is the first step and the basis in OD research. Improving IOD can improve POD and thus OD overall. This research is focused on testing a new form of IOD observations in hopes of improving the overall IOD results and subsequently OD research as whole. By acquiring improved data for IOD calculations, PODs can be further refined to obtain values closer to the true orbital parameters.

2.3.3 Space-Based and Ground-Based Optical Observations of RSOs

Observing RSOs from optical ground-based and space-based sites has different advantages and drawbacks along with specific requirements. When choosing which is best for RSO observations, there are many factors to take into consideration based on the overall goal of the mission. Ground-based observations offer a range of advantages and opportunities. Ground-based sites typically have larger apertures than space-based sites and are more sensitive [28][31]. Furthermore, there are many ground-based sites that are open and accessible for research purposes worldwide. The global distributions of these ground-based sites is useful for obtaining complete sky coverages to maximize the number of RSO observations [28][31]. Along with this, maintenance and real time solutions for issues are possible since the instruments are easily accessible. However, ground-based observations are greatly affected by weather and atmospheric conditions and are usually only useful for nighttime

observations. In multi-site observations, the regular weather and atmospheric difficulties must be considered for all locations, which likely have different conditions. Similarly, for simultaneous multi-site ground-based observations, the instrumentation at all sites must be identical and the Field of View (FOV) of these instruments must line up. Additionally, research using multiple ground-based observers uncovered that the distance between the ground observers highly affect the accuracy of the IOD [32]. Multiple ground-based sites leads to more unnecessary variables affecting IOD accuracy, since the locations of pre-established ground observation locations cannot be modified. Although ground-based observations currently have the upper hand in modern SSA research, their drawbacks may outweigh their advantages.

Conversely, space-based observations offer advantages such as immunity to atmospheric and weather conditions and are minimally affected by daylight. Space-based observations also have the ability to observe with wider angles and better flexibility, which can lead to larger amounts of data collection in comparison to ground-based observations [20]. These observers also tend to have small apertures, thus reducing their sensitivities [28][31]. Attaining a larger aperture sensor to enhance its sensitivity could be incorporated, however, this comes at an increased cost [28][31]. Space-based sites also run the risk of collisions with other RSOs or anti-satellite (ASAT) actions that could cause catastrophic setbacks and destruction [31]. Therefore, one approach for SSA space-based observations is re-purposing existing sensors on satellites such as star-trackers as discussed in Chapter 2.2.2 [7][8][9][10][28]. These star-trackers provide a cheap way to obtain observations of RSOs with all the needed information to further obtain IODs [21][22]. Thus, for single- and multi-site observations, space-based sites are preferred because they have a more flexible range of observation abilities, and have no need to consider weather or atmosphere conditions.

2.3.4 Position and Velocity Vectors to Classical Orbital Elements (COE)

While angle-only observations provide position and velocity vectors, it is sometimes easier to visualize the actual orbit of an RSO using the COEs instead. This means converting the Position vector ($\mathbf{R}$) and Velocity vector ($\mathbf{V}$) into the semi-major axis, a, eccentricity, e, inclination, i, right

ascension of the ascending node , Ω, argument of perigee, ω, and true anomaly, ν. To do so, the geocentric-equatorial coordinate system is used for RSOs, where the origin is at Earth's centre [33]. Earth's equatorial plane and principle axis, $\widehat{I}$, point's in the vernal equinox direction, γ, also known as the first point of Aries [33]. Aries is an arbitrary zero point chosen for the celestial sphere, similar to that of Greenwich, where a very distant star was first located in the Aries constellation [33]. The coordinate system can be seen in figure 5 [33].

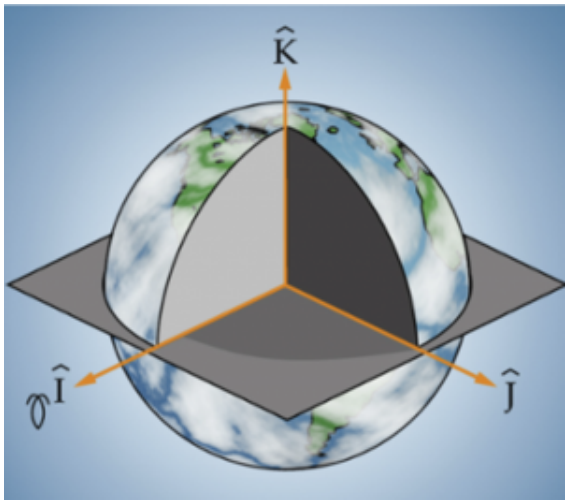

Figure 5: The geocentric equatorial coordinate frame, where $\widehat{K}$ points from the centre of Earth towards the North pole, $\widehat{I}$ points in the vernal equinox direction, γ , and $\widehat{J}$ completes the coordinate frame [33].

Semi-Major Axis a

The semi-major axis, a, describes the size of the RSO's orbit. Where, a, is half of the distance of the longest axis of the orbit, and is usually measured in kilometers (km). The size of the orbit is directly related to the specific mechanical energy, ϵ, since it is constant [33]. The total mechanical energy is the sum of the Kinetic Energy (KE) and Potential Energy (PE), while the specific mechanical energy, ϵ, is the mechanical energy divided by the mass of the object [33]. The specific Kinetic Energy, KE_s is,

$$KE_s = \frac{\mathbf{V}^2}{2}$$

PE is the mass, m, multiplied by the height, h, and the gravitational acceleration, g.

$$PE = mgh$$

Newton's Universal Law of Gravitation is then used and simplified for scenarios involving RSOs orbiting Earth [33]. Newton's Universal Law of Gravitation is,

$$F_{gravity} = \frac{Gm_{earth}m}{\mathbf{R}^2}$$

$$F_{gravity} = \frac{\mu m}{\mathbf{R}^2}$$

Where μ is Earth's gravitational parameter, which is the product of the universal gravitational constant G and the mass of the Earth m_{Earth}, with a value of $398600.5\,\text{km}^3\text{s}^{-2}$ [33]. The gravitation constant g is acting towards Earth (so a negative sign appears), and can then be expressed as,

$$F_{gravity} = -\frac{\mu m}{\mathbf{R}^2} = mg$$

$$\text{g} = -\frac{\mu}{\mathbf{R}^2}$$

Knowing this, and understanding that for potential energy, h, is equivalent to $\boldsymbol{R}$ in these scenarios, so the specific PE can be written as,

$$PE_s = \frac{mgh}{m} = -\frac{m\mu\mathbf{R}}{\mathbf{R}^2 m}$$

$$PE_s = -\frac{\mu}{\mathbf{R}}$$

The specific mechanical energy of this scenario is then [33],

$$\epsilon = KE_s + PE_s$$

$$\epsilon = \frac{\mathbf{V}^2}{2} - \frac{\mu}{\mathbf{R}}$$

It is important to note that ϵ is related to the size of the orbit, which in this case is the semi-major

axis a [33]. One way that this relationship can be derived is by starting with the assumption that the orbit is circular and then, because μ is constant, the forces can be balanced [33]. The forces in question are the centripetal force and the force of gravity,

$$F_{centrip} = \frac{\mathbf{V}^2 m}{\boldsymbol{a}}$$

$$F_{gravity} = \frac{\mu m}{\boldsymbol{a}^2}$$

Balancing these forces and solving for velocity gives,

$$\frac{\mathbf{V}^2 m}{\boldsymbol{a}} = \frac{\mu m}{\boldsymbol{a}^2}$$

$$\mathbf{V}^2 = \frac{\mu}{\boldsymbol{a}}$$

Substituting the equation for $\mathbf{V}$ shown above into the specific mechanical energy equation derived above gives,

$$\epsilon = -\frac{\mu}{2\boldsymbol{a}}$$

Although the specific mechanical energy was derived assuming the orbit was circular, the final specific mechanical energy equation is the same, even when derived from other orbital shapes [33]. The semi-major axis, a, can then easily be calculated by using the specific mechanical energy as such,

$$\epsilon = \frac{\mathbf{V}^2}{2} - \frac{\mu}{\mathbf{R}} = -\frac{\mu}{2\boldsymbol{a}}$$

Rearranging for semi-major axis a gives,

$$\mathbf{a} = -\frac{\mu \mathbf{R}}{\mathbf{V}^2 \mathbf{R} - 2\mu} \tag{1}$$

Eccentricity e

Eccentricity, e, describes the shape of the orbit, and is a unit-less quantity [33]. Eccentricity can be represented as a vector, $\boldsymbol{e}$, which points from the centre of Earth to the perigee of the orbit, and is calculated using the equation below [5][33]. The eccentricity vector equation is derived in Valldo's textbooks (Chapters 1 and 2) and is the same equation shown in George's textbook (Chapter 2)[5][33]. The variables are the same in both textbook equations, however, George uses capital letters and Vallado uses lowercase letters [5][33]. The equation for the eccentricity vector is [5][33],

$$\boldsymbol{e} = \frac{1}{\mu}[\mathbf{V} \times \boldsymbol{h}] - \frac{\mathbf{R}}{|\mathbf{R}|} \tag{2}$$

where $\boldsymbol{h}$ is the specific angular momentum vector [5][33],

$$\boldsymbol{h} = \mathbf{R} \times \mathbf{V} \tag{3}$$

The range for eccentricity and the orbit type is displayed in Table 3 [5][33].

Orbit Type	**Eccentricity Range**
Circular	$e = 0$
Elliptical	$0 < e < 1$
Parabolic	$e = 1$
Hyperbolic	$e > 1$

Table 3: The eccentricity range for the different types of orbits (unit-less) [5][33].

Inclination i

Inclination, i, describes the tilt of the orbit with respect to the $\widehat{K}$ axis and the specific angular momentum vector, $\boldsymbol{h}$, as seen in Figure 6 and has units of degrees. [33]. Where the $\widehat{K}$ vector is a unit vector that points from centre of Earth to the North pole [33].

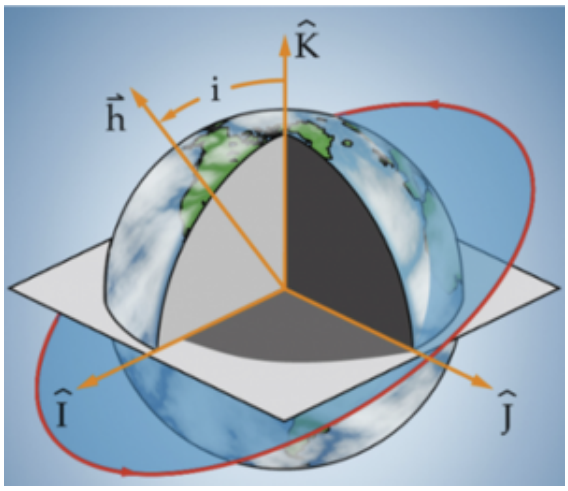

Figure 6: The geocentric equatorial coordinate frame for inclination, i [33].

The derivation of, i, can be found within Vallado's textbook (Chapter 2) and within George's textbook (Chapter 3), which starts by obtaining the angle between $\widehat{K}$ and $\boldsymbol{h}$ [5][33]. The inclination equation is seen in the equation below; where h_k is the kth coordinate of the specific angular momentum vector $\boldsymbol{h}$ [5][33].

$$i = \arccos(\frac{h_k}{|\boldsymbol{h}|}) \tag{4}$$

Right Ascension of the Ascending Node Ω

Right ascension of ascending node (**RAAN**), Ω, helps describe the orientation of the orbit in units of degrees [33]. Ω is the angle between the $\widehat{I}$ axis and the ascending node vector, $\boldsymbol{n}$; where $\boldsymbol{n}$ lies along the intersection of the orbital plane and the equatorial plane as seen in Figure 7 [33].

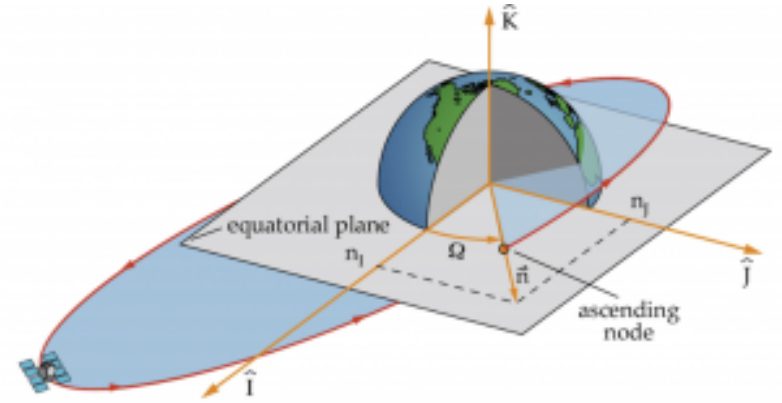

Figure 7: The geocentric equatorial coordinate frame for RAAN Ω [33].

The derivation of Ω, can be found within Vallado's textbook (Chapter 2), and within George's textbook (Chapter 3), which starts by obtaining the angle between $\widehat{I}$ and $\boldsymbol{n}$ [5][33]. The **RAAN** equation is seen in the equation below; where n_i is the ith coordinate of the ascending node vector $\boldsymbol{n}$ [5][33].

$$\Omega = \arccos\left(\frac{n_i}{|\boldsymbol{n}|}\right) \tag{5}$$

Argument of Perigee ω

Argument of perigee, ω, helps describe the orientation of the orbit in units of degrees [33]. This is the angle between the ascending node vectors $\boldsymbol{n}$ and the location of perigee where the eccentricity vector $\boldsymbol{e}$ points [33]. This orientation can be seen in Figure 8 [33].

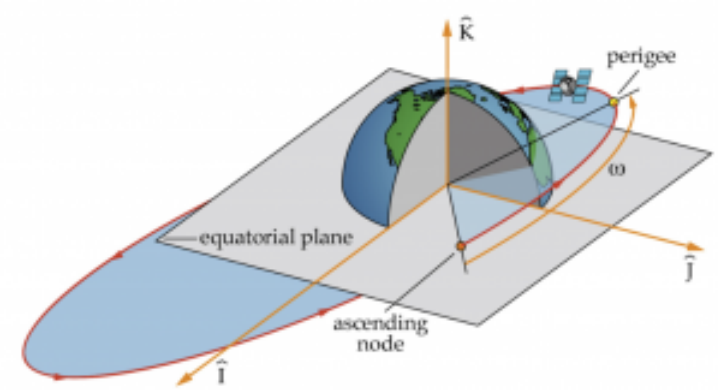

Figure 8: The geocentric equatorial coordinate frame for argument of perigee ω [33].

The derivation of, ω, can be found within Vallado's textbook (Chapter 2), and within George's textbook (Chapter 3), and begins by obtaining the angle between $\boldsymbol{n}$ and $\boldsymbol{e}$ [5][33]. The equation for argument of perigee is seen below [5][33].

$$\omega = \arccos\left(\frac{\boldsymbol{n} \cdot \boldsymbol{e}}{|\boldsymbol{n}||\boldsymbol{e}|}\right) \tag{6}$$

True Anomaly ν

True Anomaly, ν, describes the location of the object in its orbit [33] . It is the angle between the eccentricity vector $\boldsymbol{e}$ and the position vector of the satellite, $\mathbf{R}$, in units of degrees [33]. The derivation of, ν, can be found within Vallado's textbook (Chapter 2), and within George's textbook (Chapter 3), which begins by obtaining the angle between $\boldsymbol{e}$ and $\mathbf{R}$ [5][33]. The true anomaly is seen in the equation below [5][33].

$$\nu = \arccos\left(\frac{\boldsymbol{e} \cdot \mathbf{R}}{|\boldsymbol{e}||\mathbf{R}|}\right) \tag{7}$$

2.3.5 Single-Site Observations of RSOs

Single-site observations are the most common process for obtaining angles-only optical observations of RSOs, where one observational site, either ground- or space-based, is used to gather data on RSOs. For IOD, the RSO needs to be observed at three separate instances to get an arc of its orbit and for mathematical calculations of the six state vector elements of the RSO [5]. These three separate observations are obtained from the same observer, usually at different time periods. One common issue that arises from single-site observations is the too-short-arc problem due to limited data that has a high degree of similarities [29]. From single-site observational data, there are a couple of common mathematical methods used to calculate the IOD from the angle-only observations. Several common techniques used for IOD calculation are Gauss's method, Laplace's method, and Gooding's method which were described in Chapter 2.3.1 [5]. Furthermore, range measurements are not extremely accurate when using single-site observations, thus diminishing the accuracy of the IOD calculations.

2.3.6 Multi-site Observations of RSOs

Improving accuracy and precision of IOD is an ongoing focus for SSA research. The use of multi-site observations has been the topic in many future work sections within the literature with the idea that it could improve IOD accuracy and provide direct range measurement. Multi-site observations provide the ability to obtain more precise range measurements and improve IOD accuracy due to geometric differences [32][34]. When multiple observations sites, either ground- or space-based are used, data can be obtained on the same RSO without large differences in observational timing. Furthermore, multiple hosts allow for a larger range of observability, and simultaneous observations, both which benefit IOD calculations. While most IOD mathematical methods were developed for single-site observations, Gooding's method has no restriction on the configuration of the observing sites and thus can work well with different multi-site observation scenarios [14]. Its ability to process data from single- and multi-site observations made it the best option for testing this multi-site theory. Some possible advantages for multi-site observations commonly discussed within the literature include:

1. **Observational arcs:** With multiple observers, data can be taken over a longer period of time, thus decreasing the possibility of having too short of an arc for IOD calculations

2. **Simultaneous observations:** Multiple observers have the ability to obtain observation of the same RSO simultaneously, allowing for more straight forward range calculations

3. **Improved orbital accuracy:** Having more accurate range estimates as inputs for IOD algorithms allow for more accurate IOD calculations

There is significantly less research and testing done on multi-site optical observations for IOD when compared to single-site. However, the literature that does touches upon this subject and is described in Chapter 2.3.9 [9][32][34][35]. This multi-site theory is tested within this thesis in hopes of proving its ability to obtain better IOD accuracy and provide range measurements, which will further benefit SSA endeavours.

2.3.7 Obtaining RSO Range and Position Vectors from Star-trackers

The use of star-trackers for RSO detection has been studied throughout the literature and is an important starting point for further research [7][8][9][10]. This thesis takes on the next step of this star-tracker research, by using the star-tracker images as a starting point for IOD observational data. Gooding's algorithm requires an estimate of range between the host and RSO, and the Line-of-sight (LOS) unit vectors of the host [14][36][37][38][39]. These two values can be calculated using star-trackers onboard a host satellite [22]. An estimate of range can be calculated from these star-tracker images using the parallax angle; where the parallax angle is the apparent shift of an object with respect to the background [22].

Parallax is commonly used for tracking stars, or another distant natural celestial object, over long periods of time. However, it can also be used for tracking a RSO over short periods of time, as described below. For IOD research, the apparent shift is due to the host and RSO moving, and the background is the stationary stars. To calculate range, an image of the RSO needs to be taken at two different times or taken by two different observers at the same time (simultaneous observations) [22]. If the observation is taken from one observer, then the time between the two images needs to be great enough to see an actual change in movement of the RSO. Although this scenario is possible, the accuracy of the parallax calculation could suffer because one must take into consideration the movement of both the host and the RSO for that observation time range. However, if the observation is taken from two observers, then the observation can be taken simultaneously, while the observers are separated by a distance. For this scenario, only the positions of both hosts need to be accounted for, since these observations are simultaneous and do not span a time range. Regardless of the scenario, the change in the movement of the RSO in the image is called the parallax angle. For simplicity, a diagram of parallax angle for simultaneous observations is seen in Figure 10, and an example of the two images taken by two star-trackers simultaneously can be seen in Figure 9.

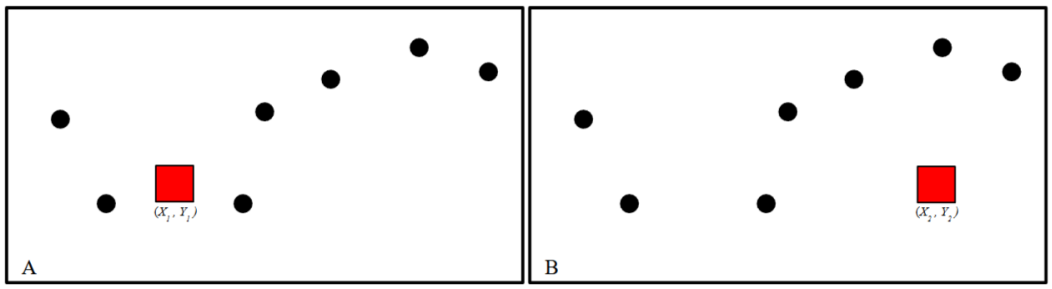

Figure 9: Example of parallax images at two times. The black dots represent background stars and red box represents the RSO being observed. Image A was taken by host 1 at time 1, where the RSO has a pixel location of (X_1,Y_1). Image B was taken by host 2 at time 1, where the RSO has a pixel location of (X_2,Y_2).

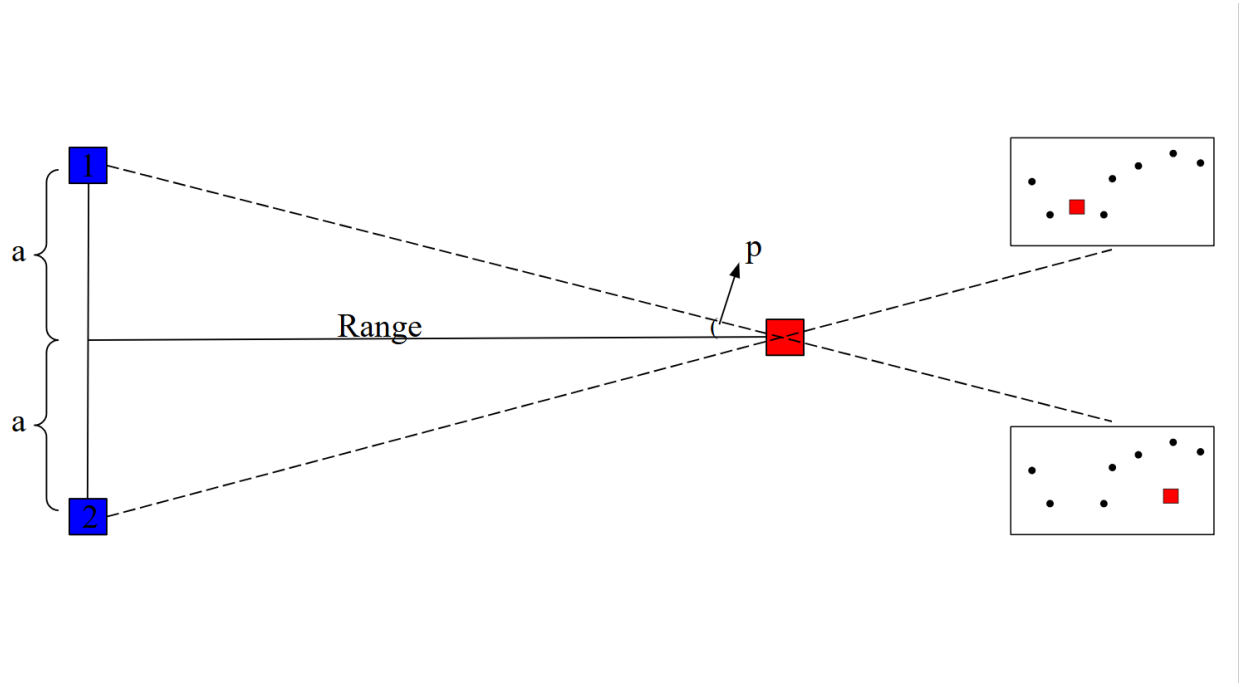

Figure 10: Parallax angle for simultaneous observations diagram. The blue box with the number '1' represents the location of host 1 at time 1. The blue box with the number '2' represents the location of host 2 at time 1. The red box represents the RSO being observed. The example parallax images from Figure 9 are shown to demonstrate what the corresponding host satellites would see at time 1. Where 'a' is the distance between one observer and the midpoints between both observers at time 1 and where 'p' is the parallax angle. 'Range' is the distance between the midpoint of the two observers and the RSO.

The equation for range using parallax angle is seen below. **Range** is the distance between the midpoint of two observers and the RSO in units of parsec. Where **a** is the distance between an observer and the midpoint between both observers in Astronomical Units (AU), and **p** is the parallax angle which is half of the total shift of the RSO between the two images in arc-seconds.

$$\textbf{Range} = \frac{a}{Tan(p)} \tag{8}$$

Using the position location (**X**,**Y**,**Z**) of both observers, the midpoint between the two locations can be approximated by simply taking the average of those two positions:

$$\textbf{Midpoint} = \frac{\begin{pmatrix}\mathbf{X}_1\\ \mathbf{Y}_1\\ \mathbf{Z}_1\end{pmatrix} + \begin{pmatrix}\mathbf{X}_2\\ \mathbf{Y}_2\\ \mathbf{Z}_2\end{pmatrix}}{2}$$

Then the vector distance between an observer and the midpoint can be approximated by subtracting one of the observers locations from the midpoint.

$$\text{Distance}_{\text{observer}} = \begin{pmatrix}\mathbf{X}_1\\ \mathbf{Y}_1\\ \mathbf{Z}_1\end{pmatrix} - \begin{pmatrix}\mathbf{X}_{midpoint}\\ \mathbf{Y}_{midpoint}\\ \mathbf{Z}_{midpoint}\end{pmatrix}$$

Finally, obtaining the magnitude of $\text{Distance}_{\text{observer}}$ gives **a**, the distance between an observer and the midpoint between both observers. It is important to note that this value of **a** is in units of kilometers and must be converted to AU.

The pixel location of the RSO in both images are needed as seen in Figure 9 $(X_1,Y_1)(X_2,Y_2)$. The distance between the two pixel locations of the RSO in the images can be calculated using the distance formula below.

$$\text{Distance}_{\text{pixels}} = \sqrt{(X_1 - X_2)^2 + (Y_1 - Y_2)^2}$$

The pixel scale of the star-tracker (in units of arc-seconds/pixel) can be used to convert $\text{Distance}_{\text{pixels}}$ to units of arc-seconds. The Fast Auroral Imager, which is the star-tracker used within this research, has a pixel scale of 382 arcseconds/pixel [13].

$$\text{Distance}_{\text{arcsec}} = \text{PixelScale}_{(\text{arcsec/pixel})} \times \text{Distance}_{\text{pixels}}$$

Since $\text{Distance}_{\text{arcsec}}$ is actually the total shift of the RSO between the two images, half of this angle is the parallax angle **p** as shown in Figure 10.

$$\mathbf{p} = \frac{\text{Distance}_{\text{arsec}}}{2} \tag{9}$$

Now that both **a** and **p** are calculated, they can be used in the **Range** equation. If range is needed as a vector, then one must simply keep values used as vectors and not scalars.

To obtain the position vector of the RSO from the image, vector addition can be followed. According to Figure 11, an estimate of the position of the RSO can be calculated by adding the position vector of the host and the range vector between the host and the RSO as seen in the equation below [22]. This can only be done if the range vector and host position vector are in the same coordinate frame. If the host is in Earth-Centered Inertial frame (ECI), and the range is not, then the range can be brought to ECI frame by taking into account the bore-sight offset; this process is described in both [22][27]. Where bore-sight offset is the distance between the center of the satellite and the center of the pointing star-tracker.

$$\mathbf{RSO_{Position}} = \begin{pmatrix} X_{Host} \\ Y_{Host} \\ Z_{Host} \end{pmatrix} + \begin{pmatrix} X_{Range} \\ Y_{Range} \\ Z_{Range} \end{pmatrix} \tag{10}$$

Where $RSO_{Position}$ is in the ECI frame [22][27]. From here, calculating the difference between $RSO_{Position}$ and the host's position, then dividing this by the **Range**, will give the LOS unit vectors needed for Gooding's IOD calculations.

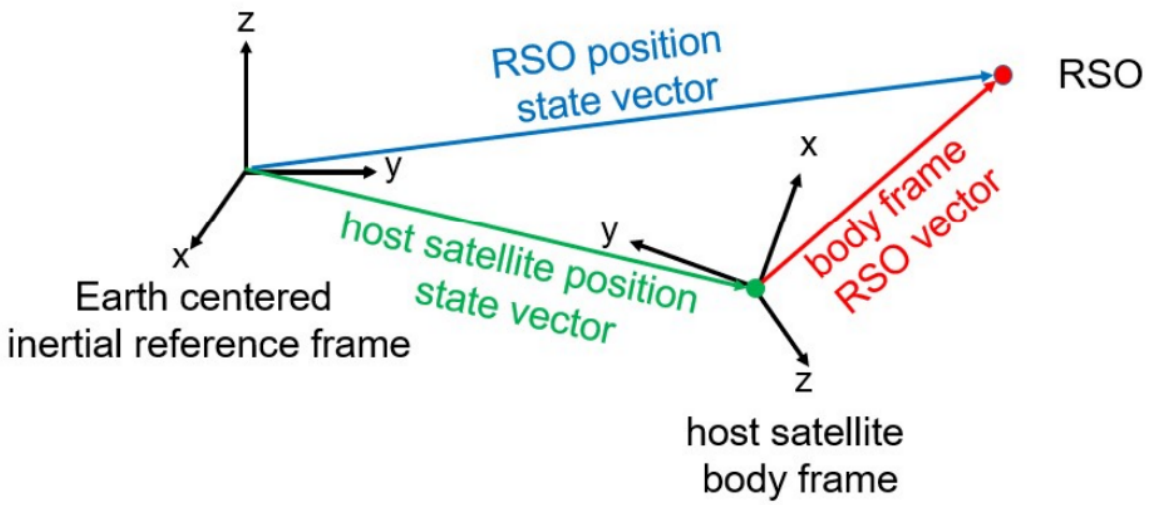

Figure 11: Vector diagram representing the calculation of the RSO position vector with respect to the host position and range vectors [22].

2.3.8 Gooding's Method

Gooding's angles-only IOD algorithm takes optical data of RSOs and calculates position and velocity vectors along with range estimates [14]. His method is chosen since it demonstrates higher precision compared to other methods, such as Gauss' method, within the literature [40][41]. Gooding's method is also said to be robust since it can process both single- and multi-site observations and covers multiple revolutions allowing data to be widely or closely spaced apart in time or position [14][40]. Furthermore, Gooding's algorithm has no restrictions for the configuration of the three observations sites, making it ideal for multi-site scenarios [14]. Due to these advantages, along with being able to iteratively solve range measurements, Gooding's algorithm is chosen for this thesis [14].

While a detailed description of Gooding's algorithm can be found in his papers, especially the formal report, his algorithm process will be briefly explained [14][36][37][38][39]. A core process in this algorithm is solving Lamberts orbital boundary-value problem, which is essentially determining the semi-major axis of an RSOs orbit using two position vectors and a time interval [14][38][42]. In simple terms; the two position vectors and time of flight are known, while the orbit

between these points are not [5]. The lambert problem is solved within Gooding's algorithm using observations as described in [14][38][40][42]. Furthermore, Lambert's original equation, for conic shape semi-major axis, can be seen in [42] and its usage is described in [14][38].

Lancaster built on Lamberts equation and made it somewhat universal so it can be used on elliptical, parabolic and hyperbolic orbits shapes, which is described and derived in [42]. Gooding's built off of Lancaster's approach to create his universal solutions for Lambert's orbital boundary-value problem as seen in [14][38]. Additionally, since two range value estimates are needed, Gooding's uses the higher-order Newton correction for solving Kepler's equations, which corrects the ranges [14][38][40][42]. Where the higher-order Newton correction is an technique which iteratively finds accurate approximations for roots in a differentiable function, which in this case is the ranges [14].

With that said, Gooding's algorithm requires various data inputs with respect to the host observer(s) along with the angles-only data of the RSO as seen in Table 4 [14][36][37][38][39]. Obtaining LOS unit vectors and range estimates from angles only data, specifically from star-trackers, is described in Chapter 2.3.7, and is important for acquiring the needed input values for Gooding's algorithm listed below. With these main inputs, Gooding's algorithm is able to produce position and velocity vectors along with refined range estimates of the RSO [14];

Inputs	Input Description	Outputs	Output Description
Time Stamps	Time duration between the first and second observation and the first and third observation	**Velocity Vector**	Velocity vector of the RSO at the second observation time in kilometers per second
Position Vectors	Position vector of host satellite at all three observation times	**Position Vector**	Position vector of the RSO at the second observation time in kilometers
Range Estimates	Initial range estimates between the host satellite and RSO at the time of the first and third observation	**Range at first observation time**	Iteratively refined range measurement between the host satellite and RSO at the first observation time
Line-of-sight	Line-of-sight unit vector of the RSO with respect to the host satellite at all three observation times	**Range at third observation time**	Iteratively refined range measurement between the host and RSO at the third observation time
Total number of main inputs	10	**Total number of outputs**	4

Table 4: Main inputs and outputs for Gooding's algorithm [14][36][37][38][39].

Gooding's algorithm for IOD research has been used and tested a number of times for a variety of scenarios, and compared against other well used IOD algorithms, which is described in Chapter 2.3.9. Gooding's algorithm, originally formatted in FORTRAN coding language, is the chosen IOD method of this thesis, which was obtained from [43] and processed in python using a FORTRAN to python install [44]. The testing of this code is explained in Chapter 3.3.

2.3.9 Related Work

IOD is a very important and challenging part of SSA research. Research in this field spans a large number of areas such as; comparing different observational approaches, like optical and radar, using

ground- or space-based observations, testing a variety of known IOD algorithms such as Gauss, Laplace and Gooding's algorithm and the use of single- or multi-site observations [5][14][20]. It is important to note that most IOD research has been done using ground-based observations and a vast majority of this was done using a single observation site [20]. This thesis is focused on using space-based observations, specifically from star-trackers, to test IOD accuracy using multi-site observations.

As previously stated, the use of star-trackers for RSO observations is currently being studied and supported, hence the use of it in this thesis [7][8][9][10]. While star-trackers have been tested for RSO detection capabilities, they have not been used extensively for IOD purposes. [9] Tests the theory for using a single star-tracker and multiple star-trackers for RSO detection and observations using a series of simulations. These simulations demonstrate that it is certainly possible, and highly encouraged, to continue in this direction of initial orbit determination research [9]. Furthermore, [35] tests the idea of using star-trackers on two different satellites in order to observe RSOs and calculate their IODs. Results from this work uses Gibbs method to calculate the IOD of RSOs observed by the two star-trackers, which seen IOD accuracy improvement when compared to using a singular host star-tracker [35]. These works further support the idea that star-trackers can be used for not only single-site, but multi-site RSO observations as well. With these observations, data such as LOS unit vectors and range can be calculated, which is essential information in obtaining IODs using Gooding's algorithm [9][14].

While [9] and [35] are some of the closet forms of space-based multi-site observation in the literature, there is other research that tests ground-based multi-site observations. A study was done using two ground-based telescopes to observe RSOs and obtain their IOD using data from both sites [32]. That research confirms that using two observation sites did improve IOD accuracy when compared to a single-site observations [32]. Although this study is done with multi-site ground-based observations, it provides strong support that multi-site observations truly can produce more accurate IOD results in certain scenarios [32]. Additionally, [34] also uses two ground-sites to observe RSOs, specifically geosynchronous satellites, for orbit determination purposes. This

research again demonstrates that using two-sites yields better initial orbit determination accuracy than single-site observations [34]. Although the research in using multi-site observation for IODs is very sparse, the idea of it is supported and encouraged in countless papers found in literature that focus on IOD improvements, some being [7][45]. Due to the lack of multi-site research for IOD purposes, this thesis is finally testing the concept of multi-site space-based observations for IOD, to see if it will significantly improve IOD accuracy.

As mentioned in a Chapter 2.3.1, some very common IOD algorithms include Laplace's method, Gauss' method, Gooding's method and more. There is a lot of research in the IOD field debating which IOD algorithm is the most robust and can produce the most accurate results. For LEO RSOs, [46] tests four IOD algorithms using artificial data: Laplace's method, Gauss' method, Double-r Iteration and Gooding's method. Various observational scenarios are tested for each of these IOD methods and Gooding's algorithm seems to be the most robust for a variety of these scenarios [46]. Additionally, [47] tests Laplace's method, Gauss' method, Baker-Jacoby's method and Gooding's method with ground-site single-site observations for objects in LEO, MEO, GEO and Highly Elliptical Orbits (HEO). From the results, again, Gooding's algorithm performs better than the rest for a large majority of observational scenarios, even the scenarios with HEOs [47]. Although there are countless scenarios in which IOD algorithms can be tested for accuracy and robustness, it is clear that within the literature, Gooding's algorithm is one of the most reliable IOD algorithms to use. Although most of these IOD algorithm comparison research is done using only single-site observations, it is believed in this thesis that Gooding's algorithm would perform the best in the space-based multi-site tested within this thesis research. It is also important to note that [9], has successfully used Gooding's method for testing their scenario IOD outcomes and thus encourages the use of Gooding's algorithm for this thesis research.

Even though space-based multi-site optical observations for IOD purposes is not highly studied within the literature, it is continuously mentioned as the direction for future research. Using the support found throughout the literature, this thesis focuses on studying space-based multi-site optical observations, and uses Gooding's method to determine if more accurate IODs can be obtained in

comparison to single-site scenarios. With the literature's support in using star-trackers for multi-site observations, and Gooding's robust algorithm, IOD accuracy can be improved in hopes to help with SSA research.

Chapter 3: Simulation Processes

3.1 Scenario Set-up and Data Collection

Publicly available space-based observations of RSOs are extremely minimal, with multi-site observations non-existent, so this thesis uses simulated scenarios created from real ephemeris and TLE data. These simulated observations were used to produce the data needed to calculate IOD using Gooding's algorithm. For all the scenarios, the simulated objects and the resulting data are deterministic, meaning that neither the simulations nor the acquired data include any measure of noise. The effects of measurement noise and the associated limitations are left for future work which is discussed in Chapter 5.3.

All hosts are modelled after the CASSIOPE satellite by using the publicly available ephemeris and sensor parameter specifications [11][13]. The onboard sensor is represented by a conical field of view (FOV) of 26°, consistent with the specifications of the Fast Auroral Imager (FAI) star tracker [13]. Observational data was obtained through a single host, two host and three hosts in order to compare IOD results between single- and multi-site observations. The multi-site configurations are limited to a maximum of three host satellites to match the three-observation input structure of Gooding's algorithm. Ten RSOs in LEO, MEO and GEO were simulated using TLEs and are propagated over time using the SGP4 propagator [12][16]. The number of RSOs was selected based on values reported in the literature, where studies typically evaluated fewer than ten objects [9][32][34][35]. Similarly, three distinct orbits were chosen, since recent literature focused on RSOs within only a singular orbit [9][32][34][35]. The number of RSOs and orbits considered in this thesis were intentionally chosen to provide a more comprehensive analysis and extend beyond the scope of previous literature.

Nine different scenarios were evaluated, each designed to address one or more of the research objectives outlined in Chapter 1.2. For all scenarios, the RSO set, observation dates, and observation times are held constant to ensure consistent and directly comparable results. The estimated position, velocity, and range variables from each scenario are evaluated against STK truth data to determine

which configuration produces the most accurate IOD results.

The four main steps for the overall data collection, which are described in detail within the following subchapters, are [11][13][16][43][44][48]:

1. **Simulation:** Create single-site and multi-site simulations
2. **Access reports:** Obtain access reports from the hosts and RSOs for all scenarios
3. **LOS unit vectors and range calculation:** Calculate the LOS unit vectors and range estimate from the access reports
4. **Gooding's Algorithm:** Use the LOS unit vectors, range, and other input values for Gooding's algorithm to obtain IODs of the RSOs

3.2 Ansys System Tool Kit (STK)

Since there is no public observational data readily available, the Ansys System Tool Kit (STK) is used as a tool to create all single- and multi-site observations and generate the input data needed for IOD calculations [12]. These visual simulations ensure that the scenarios being studied are logical and realistic; such as ensuring hosts and RSOs are not crashing down into Earth or flying off into deep space. STK additionally serves as the source of truth state vectors for all RSOs, against which the IOD outputs are evaluated for accuracy [12]. For all scenarios, access reports are obtained for each RSO. Access reports contain information on when the RSO is in the FOV of the host's sensor and provides the information needed to calculate IOD, such as host position vectors and time intervals [12]. This data does not include noise measurements. However, future work should incorporate noise measurements and its impact on the results, as discussed in Chapter 5.3.

Orientations for both single- and multi-site observations were configured using CASSIOPE's ephemeris data which uses the geocentric equatorial inertial frame [11]. The three main orientations tested within this research are; single-site, multi-site straight line, and multi-site diagonal line as seen in Figure 12 and explained throughout this Chapter. All host in every scenario are located in

LEO to support the idea that star-tracker imagers can be used for collecting IOD observational data [1][7][8][9][10].

The nine scenarios evaluated in this thesis are:

1. **Single-site:** Observations done $\geq 300sec$
2. **Normal 2-site straight line (SL):** Observations done $\geq 300sec$
3. **Simultaneous (SIM) 2-site SL:** Observations done $\leq 40sec$
4. **Normal 2-site diagonal line (DL):** Observations done $\geq 300sec$
5. **SIM 2-site DL:** Observations done $\leq 40sec$
6. **Normal 3-site SL:** Observations done $\geq 300sec$
7. **SIM 3-site SL:** Observations done $\leq 40sec$
8. **Normal 3-site DL:** Observations done $\geq 300sec$
9. **SIM 3-site DL:** Observations done $\leq 40sec$

For all multi-site scenarios, with either two or three host, and in either the straight or diagonal line scenario, data from the access reports were taken for observations done 'simultaneously' and 'normally'. The *normal* observations for all scenarios in this thesis, single- or multi-site, where all $\geq 300sec$ apart. *Normal* observations are done over this time range to ensure that a large enough observational arc is obtained for all three orbits, reducing the possibility of a too-short-arc. This is intentional so that time constraints and changes for each of the 30 RSOs are not sporadic, making comparisons between multi- and single-site observations more straightforward.

For multi-site scenarios, *simultaneous* observations are possible since numerous hosts can observe an RSO at the same time. For all of the multi-site scenarios the *simultaneous* observations were $\leq 40sec$ apart. The lower bound for *simultaneous* observations are not always zero due to simulation constraints and the practical difficulty of achieve perfect synchronization across the

multiple hosts [12]. However, this is consistent with real operational scenarios, in which truly simultaneous multi-site observations are rarely achievable due to geometric and technological limitations.

The major comparison for this thesis is to see if multi-site observations as a whole are more accurate than single-site observations. So, for the sake of consistency, observational times had to be long enough so that a large enough observation arc of GEO RSOs could be obtained. Nonetheless, these two different types of observations are useful for testing the accuracy of single- vs multi-site observations and to see if, for multi-site scenarios, *simultaneous* observations produce higher IOD accuracy than *normal* observations.

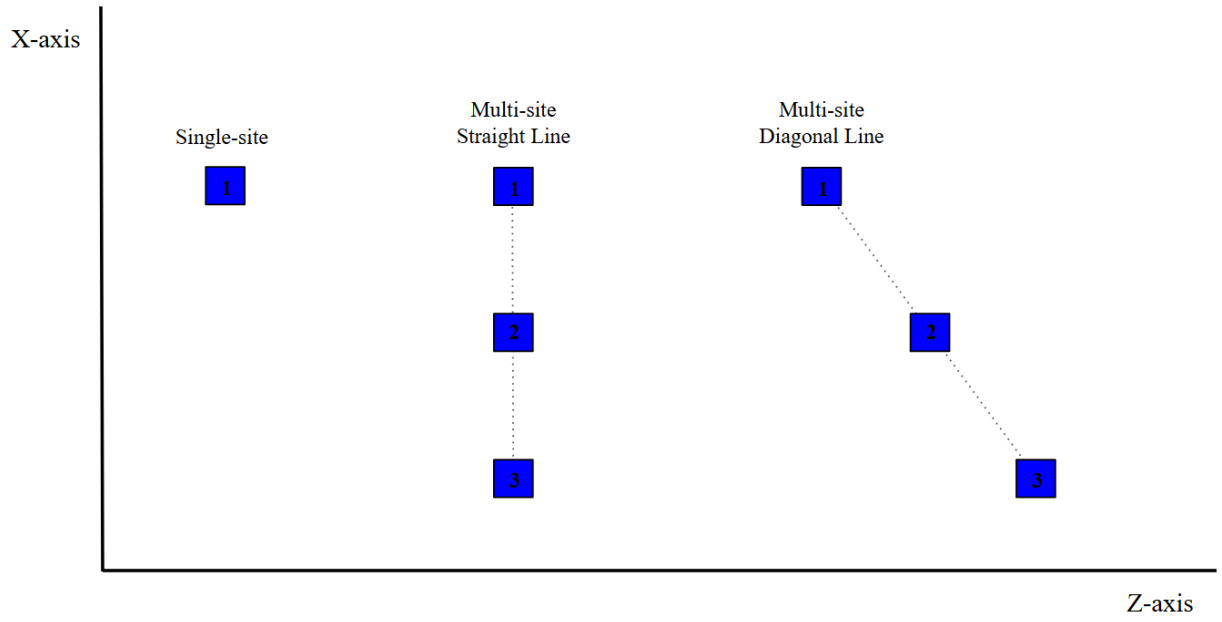

Figure 12: All three orientations for host satellites that are tested in this research: single-site, multi-site straight line, and multi-site diagonal line.

3.2.1 Ansys System Tool Kit Single-site Scenarios

Single-site observations only contain one host, which is simulated using the original ephemeris data, with no added orbital changes. By using ephemeris and TLE data, both the host and RSO states are grounded in real observational data. While the single-site orientation can be seen in

Figure 12, the simulation can be seen in Figure 13 and Figure 14 [12].

A step by step breakdown of the single-site simulation and data collection process can be seen below [11][12][13][16]:

- **Simulation process**

    1. Obtain ephemeris data for CASSIOPE host satellite from epop website
    2. Upload ephemeris file into STK to simulate the CASSIOPE host satellite (referred to as 'CASSIOPE' in Figure 13)
    3. Add sensor to CASSIOPE
    4. Simulate 30 known RSOs (10 found in LEO, 10 found in MEO, and 10 found in GEO) using STK's built in SGP4 propagator

- **Data collection process**

    1. Obtain access report between CASSIOPE and the 30 RSOs (will have 30 access reports total)
    2. Choose an access interval time range from the access report (this remained consistent for all simulations, single- or multi-site, to ensure easy and fair comparisons)
    3. Choose three specific times from the access interval time range to use as input data

The data from the access reports was used as input data for Gooding's algorithm, which is described in Chapter 3.3 [12][14].

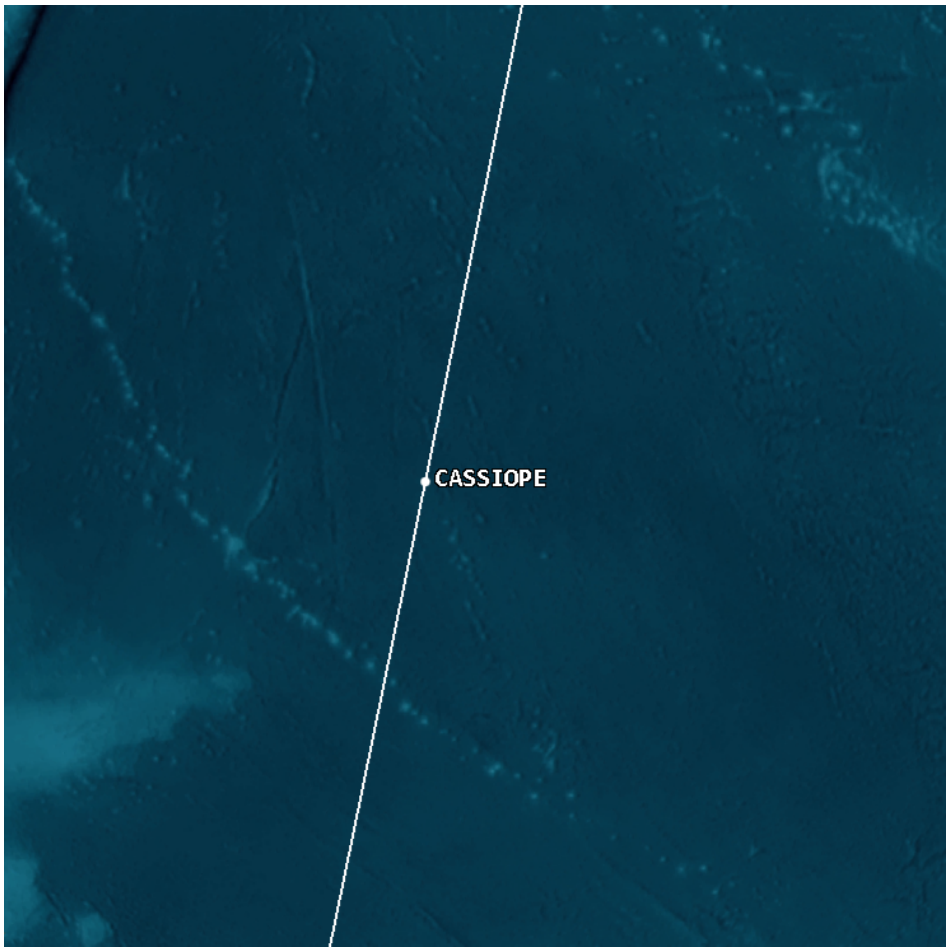

Figure 13: STK simulation of the single-site host. The movement of the host is going from the top of image to bottom of image [11][12][13].

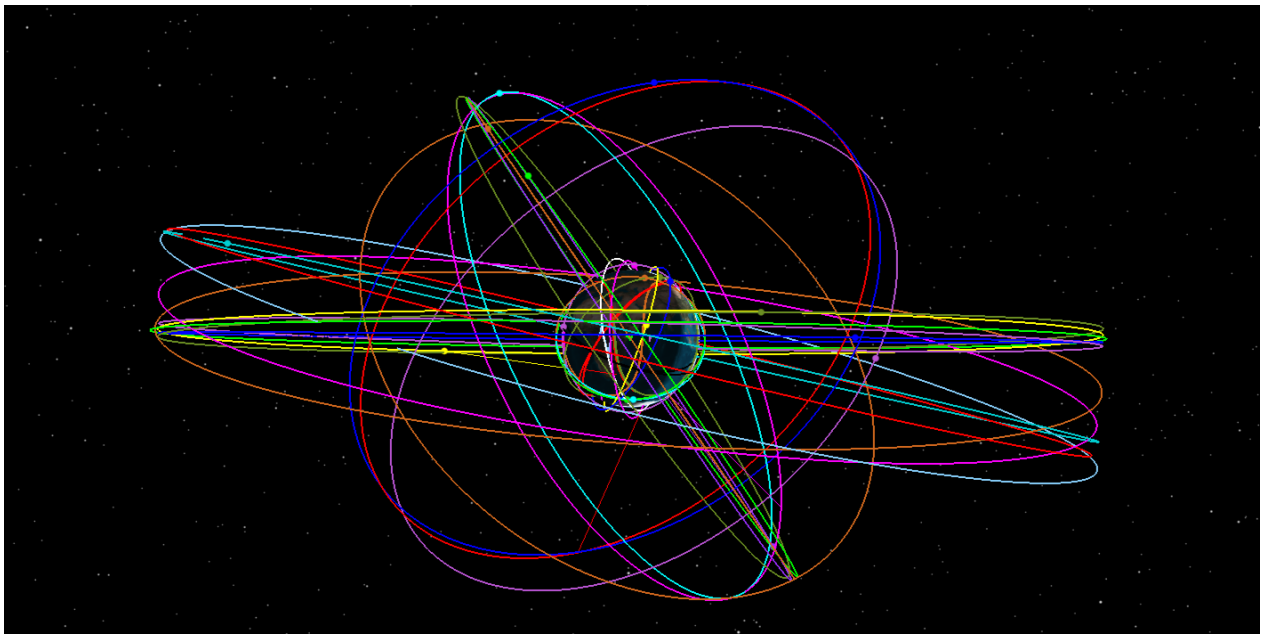

Figure 14: STK simulation of the single-site host and all 30 RSOs [11][12][13].

3.2.2 Ansys System Tool Kit Multi-site Scenarios

Subsequently, the multi-site scenarios involved using two and three host satellites. By using ephemeris and TLE data, all the hosts and RSO states are grounded in real observational data. Since IOD algorithms, such as Gooding's algorithm, requires only three observations of a RSO, a maximum of three host satellites were simulated [11][12]. Therefore, including additional hosts for this research would be redundant. The multi-site scenarios were oriented in two different ways: in a straight line or in a diagonal line. Both orientations can be seen along with the single-site host in Figure 12. These orientations were chosen as a baseline since they form a simple yet physically distinct baseline for formation flying IOD research, providing an initial reference for future mission design studies. Additionally, the separation between the hosts was chosen to ensure that all FOVs had some overlap to provide *simultaneous* observations.

Straight Line Scenario

The first host satellite in the Straight Line scenario (SL) was simulated identically to the single-site host in Chapter 3.2.1 [11][12][13][16][48]. The second and third host satellites are derived

from the same ephemeris, with their state vectors propagated forward in time by 10 s and 20 s respectively relative to the first host satellite. CASSIOPE's mean orbital speed is approximately 7.5 km/s, meaning the 10 s and 20 s time propagation correspond to along-track separations of approximately 75 km and 150 km in the X-axis, placing all three hosts in a collinear formation as illustrated in Figure 15.

Data was obtained through access reports as described in Chapter 3.2.1, the only difference being that the access report came from two or three hosts instead of just one [12]. So for clarity, the scenario for two hosts only took data (access reports) from the original host and the second host, while the scenario for three hosts took data (access reports) from all three hosts. The step by step breakdown for the straight line multi-site scenario is outlined below and can be seen in Figure 15 and Figure 17 [12].

- **Simulation process**

    1. Obtain ephemeris data for CASSIOPE host satellite from epop website
    2. Upload ephemeris file into STK to simulate the CASSIOPE host satellite (referred to as 'CASSIOPE_1' in Figure 15)
    3. Add sensor to CASSIOPE_1
    4. Duplicate the original ephemeris file from CASSIOPE_1 and propagate it ahead in time by 10 seconds
    5. Upload the adjusted ephemeris file into STK to simulate the second CASSIOPE host satellite (referred to as 'CASSIOPE_2' in Figure 15)
    6. Add sensor to CASSIOPE_2
    7. Duplicate the original ephemeris file from CASSIOPE_1 and propagate it ahead in time by 20 seconds
    8. Upload the adjusted ephemeris file into STK to simulate the third and final CASSIOPE host satellite (referred to as 'CASSIOPE_3' in Figure 15)

9. Add sensor to CASSIOPE_3
10. Simulate 30 known RSOs (10 found in LEO, 10 found in MEO, and 10 found in GEO) using STK's built in SGP4 propagator

- **Data collection process**

1. Obtain access report between CASSIOPE_1 and the 30 RSOs , CASSIOPE_2 and the 30 RSOs, and CASSIOPE_3 and the 30 RSOs (will have 90 access reports total)
2. Choose an access interval time range from the access report (this remained consistent for all simulations, single- or multi-site, to ensure easy and fair comparisons)
3. **For two-site *normal* observations**: Choose three specific times from the access interval time range to use as input data. Since there are two different access reports for an individual RSO, data will be taken from both access reports
4. **For two-site *simultaneous* observations**: Choose one specific time from the access interval time range to use as input data. Since there are two different access reports for an individual RSO, data will be taken from both access reports
5. **For three-site *normal* observations**: Choose three specific times from the access interval time range to use as input data. Since there are three different access reports for an individual RSO, data will be taken from all access reports
6. **For three-site *simultaneous* observations**: Choose one specific time from the access interval time range to use as input data. Since there are three different access reports for an individual RSO, data will be taken from all access reports

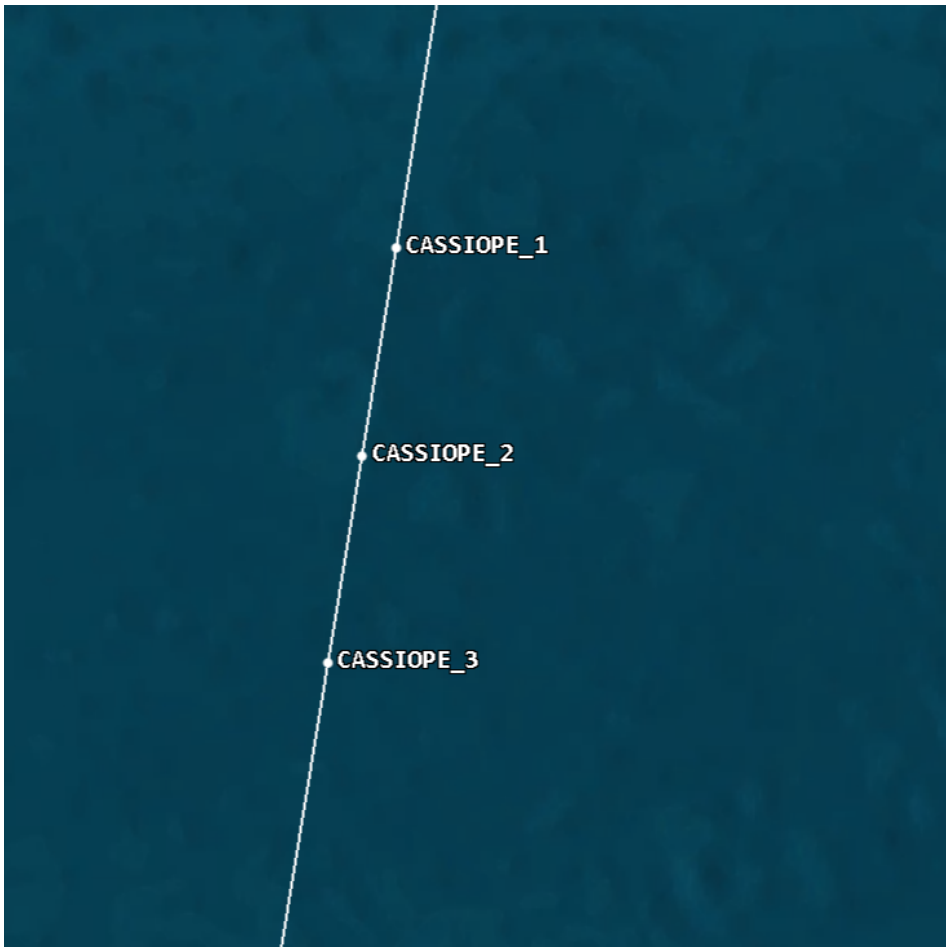

Figure 15: STK simulation of the straight line multi-site scenarios with two and three hosts. The movement of all hosts are going from the top of image to bottom of image [11][12][13].

Diagonal Line Scenario

The first host satellite in the Diagonal Line scenario (DL) was simulated identically to the single-site host in Chapter [11][12][13][16][48]. The second and third host satellites are derived from the same ephemeris and adjusted accordingly [11][13][49]. The second satellite was propagated by 10 km in the X axis and by 5 km in the Z axis while the third satellite was propagated by 20 km in the X axis and by 10 km in Z axis. These offsets produced a diagonal line as illustrated in Figure 16 [12].

Data was obtained through access reports in the same matter described in the SL scenario. The step by step breakdown for the diagonal line multi-site scenario is outlined below and the simulations can be seen in Figure 16 and Figure 17 [12]. Furthermore, an example of access reports

and data collection for all scenarios are seen and discussed in 3.3.1.

- **Simulation process**

  1. Obtain ephemeris data for CASSIOPE host satellite from epop website
  2. Upload ephemeris file into STK to simulate the CASSIOPE host satellite (referred to as 'CASSIOPE_1' in Figure 16)
  3. Add sensor to CASSIOPE_1
  4. Duplicate the original ephemeris file from CASSIOPE_1 and propagate it by 10 km in the X axis and by 5 km in the Z axis
  5. Upload the adjusted ephemeris file into STK to simulate the second CASSIOPE host satellite (referred to as 'CASSIOPE_2' in Figure 16)
  6. Add sensor to CASSIOPE_2
  7. Duplicate the original ephemeris file from CASSIOPE_1 and by 20 km in the X axis and by 10 km in the Z axis
  8. Upload the adjusted ephemeris file into STK to simulate the third and final CASSIOPE host satellite (referred to as 'CASSIOPE_3' in Figure 16)
  9. Add sensor to CASSIOPE_3
  10. Simulate 30 known RSOs (10 found in LEO, 10 found in MEO, and 10 found in GEO) using STK's built in SGP4 propagator

- **Data collection process**

  1. Obtain access report between CASSIOPE_1 and the 30 RSOs , CASSIOPE_2 and the 30 RSOs, and CASSIOPE_3 and the 30 RSOs (will have 90 access reports total)
  2. Choose an access interval time range from the access report (this remained consistent for all simulations, single- or multi-site, to ensure easy and fair comparisons)

3. **For two-site *normal* observations**: Choose three specific times from the access interval time range to use as input data. Since there are two different access reports for an individual RSO, data will be taken from both access reports
4. **For two-site *simultaneous* observations**: Choose one specific time from the access interval time range to use as input data. Since there are two different access reports for an individual RSO, data will be taken from both access reports
5. **For three-site *normal* observations**: Choose three specific times from the access interval time range to use as input data. Since there are three different access reports for an individual RSO, data will be taken from all access reports
6. **For three-site *simultaneous* observations**: Choose one specific time from the access interval time range to use as input data. Since there are three different access reports for an individual RSO, data will be taken from all access reports

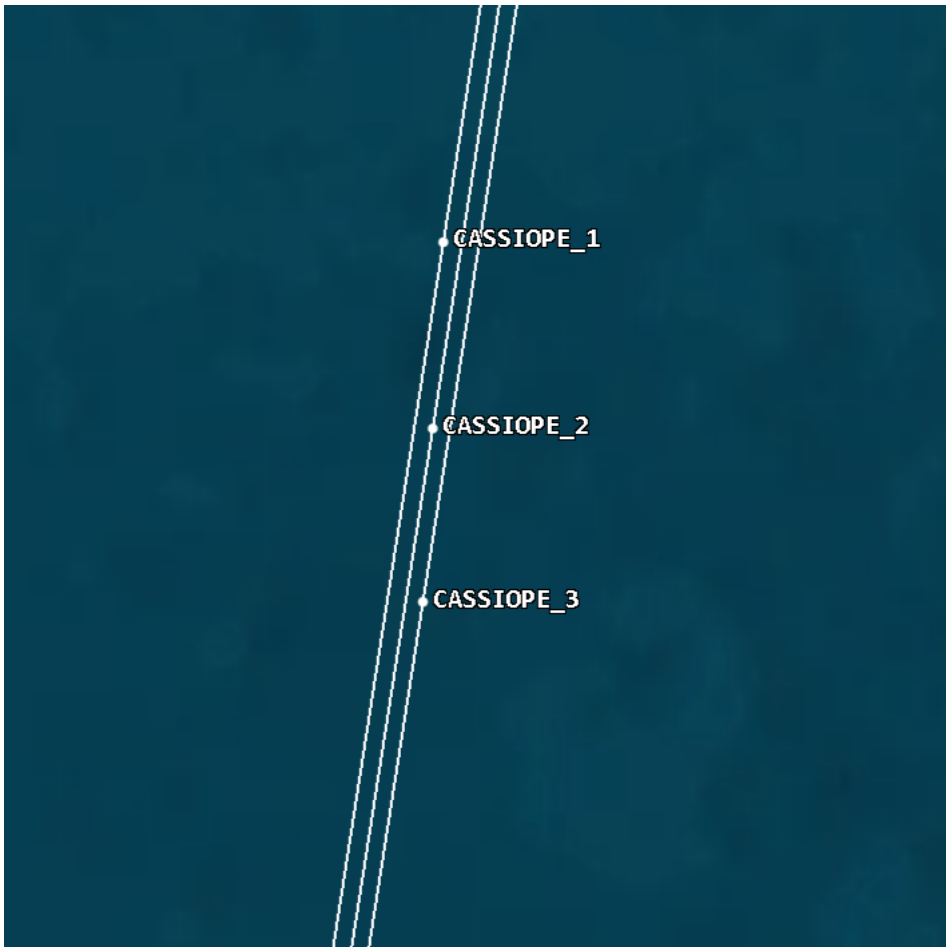

Figure 16: STK simulation of the diagonal line multi-site scenarios with two and three hosts. The movement of all hosts are going from the top of image to bottom of image [11][12][13].

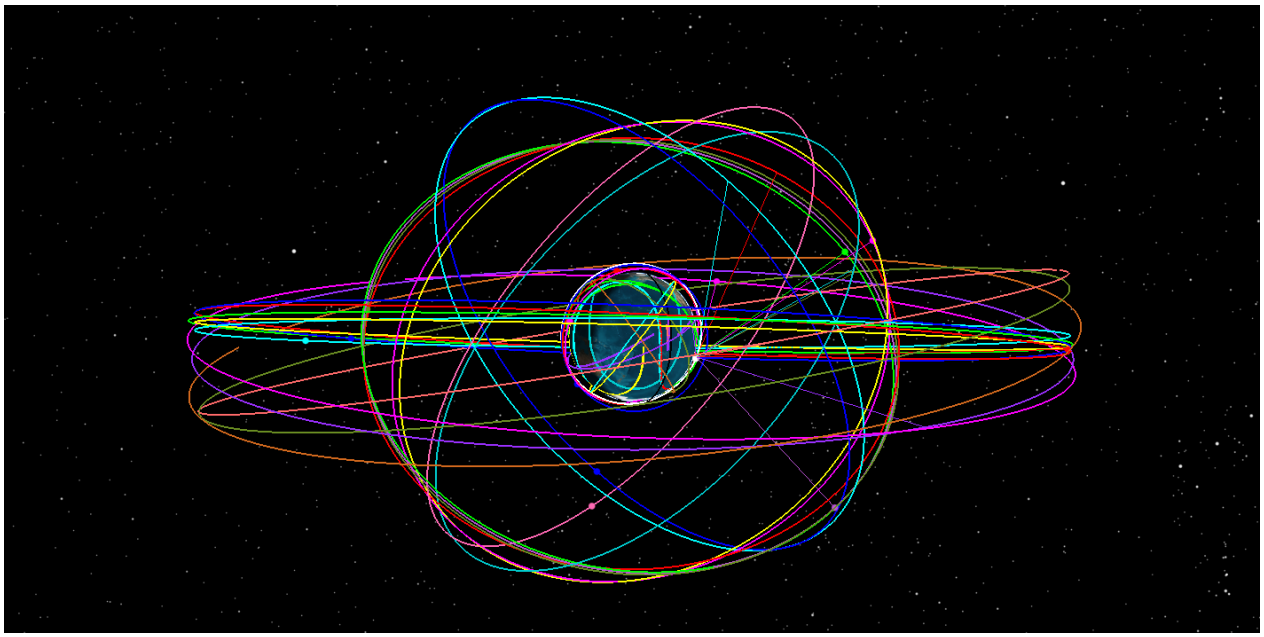

Figure 17: STK simulations of all multi-site hosts for both the straight and diagonal line scenarios, along with all 30 RSOs [11][12][13].

3.3 Gooding's Algorithm Using Single- and Multi-site Data

As explained previously, Gooding's algorithm requires a variety of input data about both the host and the RSO. Additionally, it is noted that for IOD calculations, three observations of the same RSO are needed [5]. Gooding's algorithm requires the LOS unit vectors of the RSO, the host position vector and the time from three separate observations, along with range estimate from the first and last observation [14]. For single-site observations, the three separate observations would be taken from the same host. For multi-site observations, the three separate observations comes from numerous hosts (two or three depending on the scenario in question).

With that said, it is important to explain how Gooding's algorithm was obtained. Gooding wrote his IOD algorithm in FORTRAN coding language, and a detailed description of the full IOD process is described in detail in his various papers [14][36][37][38][39]. His FORTRAN IOD algorithm was obtained from [43]. The creator of this open-source Gooding's code tested the accuracy of his code by reproducing the results of Gooding's 1993 report [14][43]. Within the

open-source code package, testing input data is provided, along with the expected correct output results, to allow the user to test the downloaded code and make sure the same outputs are produced [43]. For this thesis, python via Google Collab, was used along with a python installation which reads and runs codes written in FORTRAN [43][44]. This allowed Gooding's FORTRAN code, to be run and edited in Python for easier use [43][44]. To ensure that python was properly reading the open-source Gooding's FORTRAN code, the input data that was provided in the open source package was processed through the Python Gooding's code to test its outputs [43][44]. The python Gooding's code was able to properly process the input data and produce the correct outputs that were provided with the installation [43][44]. Thus, this open source online code was tested successfully and used for the Gooding IOD calculation portion of this thesis [43][44].

3.3.1 Access Reports

The access reports from the scenarios, from either single- or multi-site, *normal* or *simultaneous* observations, provide the needed input information for Gooding's algorithm to obtain the IOD of the RSOs [12][14][36][37][38][39]. An access report displays data for each interval of time where the host satellite had observational access of the RSO [12]. It consists of many lines of data that span the entire time range [12]. Since the access reports are very large, and the time ranges also long, Table 5 to Table 9 only display the lines of data that were actually used for analysis for that specific scenario and RSO [12]. These tables display real data of RSO 15773, which is a RSO in LEO, to help clarify what data was included in the access reports and how it was used for further IOD analysis.

Table 5 displays the access report data on RSO 15773 from the single-site scenario. Three separate observations of RSO 15773 where taken from the same host satellite, and the data from the access report for these three observations are shown in Table 5. Similarly, this same RSO was observed using the multi-site straight line scenario where three separate observations of RSO 15773 where taken from either two or three different host satellites, as seen in Table 6 and Table 7. Finally, the same RSO was observed using the multi-site diagonal line scenario where the three separate

observations of RSO 15773 where taken from either two or three different host satellites, as seen in Table 8 and Table 9. Table 5 to Table 9 display two sets of observations; the *normal* observations (in green) and the *simultaneous* observations (in yellow). Table 5 to Table 9 show an example for just one RSO; this data collection process is repeated for all 30 RSOs.

Access reports provide input data for the position of both the host and the RSO. The LOS unit vectors and range between the two objects are then calculated from the access reports [14][36][37][38][39]. This process and an example is explained in Chapter 3.3.2.

Host	Observation	Time (HMS)	Host Position X (km)	Host Position Y (km)	Host Position Z (km)	RSO Position X (km)	RSO Position Y (km)	RSO Position Z (km)
CASSIOPE	1	08:09:25	-6727.4	-590.23	-2349.7	-2292.1	1802.7	-6559.4
CASSIOPE	2	08:17:24	-4540.3	-967.44	-5164.4	-4556.5	-695.00	-5489.0
CASSIOPE	3	08:24:48	-1423.6	-1087.5	-6547.1	-5673.8	-2871.8	-3291.3

Table 5: Example of single-site scenario data from access report. This data is for the LEO RSO 15773 and is for single-site observation. The order of observations is dependent on observation time, so it is listed chronologically. The green lines represent *normal* observations [11][12][13].

Host	Observation	Time (HMS)	Host Position X (km)	Host Position Y (km)	Host Position Z (km)	RSO Position X (km)	RSO Position Y (km)	RSO Position Z (km)
CASSIOPE_1	1	08:09:25	-6727.4	-590.23	-2349.7	-2292.1	1802.7	-6559.4
CASSIOPE_2	2	08:17:29	-4570.5	-964.69	-5140.9	-4575.0	-721.22	-5470.0
CASSIOPE_3	3	08:25:00	-1491.6	-1087.7	-6534.5	-5687.0	-2920.4	-3224.8
CASSIOPE_1	1	08:18:24	-4167.7	-998.25	-5433.2	-4770.8	-1008.2	-5251.7
CASSIOPE_2	2	08:18:29	-4199.4	-995.84	-5411.7	-4787.8	-1034.2	-5231.0
CASSIOPE_3	3	08:18:33	-4237.4	-992.92	-5385.7	-4801.3	-1054.9	-5214.3

Table 6: Example of multi-site straight line with three host scenario data from access report. This data is for the LEO RSO 15773 and is for three-site straight line observations. The order of hosts is dependent on observation time so the host were listed chronologically; according from which host saw the RSO first and which host saw it last. The green lines represent *normal* observations while the yellow lines represent *simultaneous* observations [11][12][13].

Host	Observation	Time (HMS)	Host Position X (km)	Host Position Y (km)	Host Position Z (km)	RSO Position X (km)	RSO Position Y (km)	RSO Position Z (km)
CASSIOPE_1	1	08:09:25	-6727.4	-590.23	-2349.7	-2292.1	1802.7	-6559.4
CASSIOPE_2	2	08:17:29	-4570.5	-964.69	-5140.9	-4575.0	-721.22	-5470.0
CASSIOPE_2	3	08:24:54	-1457.5	-1087.6	-6540.8	-5680.5	-2896.2	-3258.0
CASSIOPE_1	1	08:18:24	-4167.7	-998.25	-5433.2	-4770.8	-1008.2	-5251.7
CASSIOPE_2	2	08:18:29	-4199.4	-995.84	-5411.7	-4787.8	-1034.2	-5231.0
CASSIOPE_2	3	08:18:29	-4199.4	-995.84	-5411.7	-4787.8	-1034.2	-5231.0

Table 7: Example of multi-site straight line with two host scenario data from access report. This data is for the LEO RSO 15773 and is for two-site straight line observations. The order of hosts is dependent on observation time so the host were listed chronologically; according from which host saw the RSO first and which host saw it last. The green lines represent *normal* observations while the yellow lines represent *simultaneous* observations [11][12][13].

Host	Observation	Time (HMS)	Host Position X (km)	Host Position Y (km)	Host Position Z (km)	RSO Position X (km)	RSO Position Y (km)	RSO Position Z (km)
CASSIOPE_3	1	08:09:21	-6738.9	-590.80	-2351.0	-2275.3	1817.7	-6561.1
CASSIOPE_2	2	08:17:23	-4542.0	-968.38	-5169.9	-4552.8	-689.75	-5492.7
CASSIOPE_1	3	08:24:48	-1423.6	-1087.5	-6547.1	-5673.8	-2871.8	-3291.3
CASSIOPE_3	1	08:16:21	-4903.5	-933.76	-4879.2	-4312.4	-363.17	-5715.1
CASSIOPE_2	2	08:16:23	-4895.6	-933.44	-4878.8	-4320.5	-373.73	-5708.3
CASSIOPE_1	3	08:16:24	-4893.5	-932.51	-4873.4	-4324.5	-379.01	-5704.9

Table 8: Example of multi-site diagonal line with three host scenario data from access report. This data is for the LEO RSO 15773 and is for three-site diagonal line observations. The order of hosts is dependent on observation time so the host were listed chronologically; according from which host saw the RSO first and which host saw it last. The green lines represent *normal* observations while the yellow lines represent *simultaneous* observations [11][12][13].

Host	Observation	Time (HMS)	Host Position X (km)	Host Position Y (km)	Host Position Z (km)	RSO Position X (km)	RSO Position Y (km)	RSO Position Z (km)
CASSIOPE_3	1	08:09:21	-6738.9	-590.80	-2351.0	-2275.3	1817.7	-6561.1
CASSIOPE_2	2	08:17:23	-4542.0	-968.38	-5169.9	-4552.8	-689.75	-5492.7
CASSIOPE_2	3	08:24:49	-1412.5	-1088.3	-6554.4	-5674.2	-2873.1	-3289.5
CASSIOPE_3	1	08:16:21	-4903.5	-933.76	-4879.2	-4312.4	-363.17	-5715.1
CASSIOPE_2	2	08:16:23	-4895.6	-933.44	-4878.8	-4320.5	-373.73	-5708.3
CASSIOPE_2	3	08:16:23	-4895.6	-933.44	-4878.8	-4320.5	-373.73	-5708.3

Table 9: Example of multi-site diagonal line with two host scenario data from access report. This data is for the LEO RSO 15773 and is for two-site diagonal line observations. The order of hosts is dependent on observation time so the host were listed chronologically; according from which host saw the RSO first and which host saw it last. The green lines represent *normal* observations while the yellow lines represent *simultaneous* observations [11][12][13].

3.3.2 LOS and Range Calculations Using Simulated Data

The process of calculating LOS unit vectors and range is identical in all scenario events. An example calculation for just the first observation in Table 5 is outlined below [12]. Table 10 displays all the LOS and range values calculated from Table 5 along with the remaining inputs values and is explained in Chapter 3.3.3. It is important to note that the process used for calculating range and LOS unit vectors is done this way since simulated data is used [12]. However, the range and LOS calculations outlined in Chapter 2.3.7 would be used for real star-tracker observation, and used instead of the process outlined below.

The LOS unit vectors and range between the host and RSO is calculated using the data obtained from the access reports. The first step is to compute the relative position vector, P. This is done by subtracting the host position from the RSO position.

The subtraction of the two position vectors can be written as:

$$P = \begin{pmatrix} x_{RSO} \\ y_{RSO} \\ z_{RSO} \end{pmatrix} - \begin{pmatrix} x_{Host} \\ y_{Host} \\ z_{Host} \end{pmatrix}$$

$$P = \begin{pmatrix} -2292.1 \\ 1802.7 \\ -6559.4 \end{pmatrix} km - \begin{pmatrix} -6727.4 \\ -590.23 \\ -2349.7 \end{pmatrix} km$$

$$P = \begin{pmatrix} 4435.3 \\ 2393.0 \\ -4209.7 \end{pmatrix} km$$

The range, **R**, between the host and RSO was then found by calculating the norm (the magnitude) of the relative position vector just calculated:

$$\|\mathbf{R}\| = \sqrt{P_x^2 + P_y^2 + P_z^2} km$$

$$\|\mathbf{R}\| = \sqrt{(4435.3)^2 + (2393.0)^2 + (-4209.7)^2} km$$

$$\|\mathbf{R}\| = 6566.5 km$$

Lastly, to obtain the LOS unit vectors, **LOS**, the relative position vector is divided by the range:

$$\mathbf{LOS} = \frac{1}{6566.5 km} \begin{bmatrix} 4435.3 \\ 2393.0 \\ -4209.7 \end{bmatrix} = \begin{bmatrix} 0.67543 \\ 0.36441 \\ -0.64107 \end{bmatrix}$$

These steps would be repeated for all three observation of the RSO for all of the simulations, single- and multi-site, *normal* observations and *simultaneous* observations [11][12][13]. From there, the times, host position, LOS unit vectors, and estimated range values are used as inputs for Gooding's algorithm [14][36][37][38][39]. As stated before, with these main inputs, and a variety of other constants, Gooding's algorithm takes these observations and outputs the position and velocity vectors of the RSO at the second observation time and the range values for the first and third observation times [14][36][37][38][39]. An example of the input and output values for this process is shown in Chapter 3.3.3. Once all the results are obtained for all RSOs for each scenario,

the bias, standard deviation, and root mean square error can be calculated using the data points (position, velocity, range) directly from STK as truth data and the calculated results from Gooding's algorithm output [12][14][36][37][38][39]. This allows for an IOD accuracy comparison between all the single- and multi-site observations. The results and analysis is described in detail in the Chapter 4.

3.3.3 Final Input Values for Gooding's Algorithm

With the data obtained, the LOS unit vectors and range values calculated, all the main input values for Gooding's algorithm were obtained. As stated in Chapter 2.3.8 the main inputs for Gooding's algorithm consists of time, position vector of the host, LOS unit vectors of the RSO and estimated range values [14]. From here, these values are used as input for Gooding's algorithm, and the IOD for the RSOs can be obtained [14][43]. Where the IOD consists of position vectors, velocity vectors, and range estimates of the RSO with respect to the host satellite(s) [14]. Using the data from Table 5 and the example calculations from Chapter 3.3.2, a full example of the main inputs and the outputs for Gooding's algorithm can be seen in Table 10 and Table 11 [14][43].

Inputs	**Input Value**
Time between first and second observation (s)	479.00
Time between first and third observation (s)	923.00
Position vector of host at time 1 (km)	(-6727.4, -590.23, -2349.7)
Position vector of host at time 2 (km)	(-4540.3, -967.44, -5164.4)
Position vector of host at time 3 (km)	(-1423.6, -1087.5, -6547.1)
LOS unit vector of RSO at time 1	(0.67543, 0.36441, -0.64107)
LOS unit vector of RSO at time 2	(-0.038245, 0.64240, -0.76540)
LOS unit vector of RSO at time 3	(-0.75312, -0.31617, 0.57691)
Range estimate at time 1 (km)	6566.5
Range estimate at time 3 (km)	5643.4

Table 10: Example of the **MAIN** inputs for Gooding's algorithm from LEO single-site observations of RSO 15773 [14].

Output	**Output Value**
Position vector of RSO at time 2 (km)	(-4556.4, -696.98, -5486.6)
Velocity vector of RSO at time 2 (km/s)	(-3.6345, -5.2098, 3.7070)
Range estimate at time 1 (km)	6507.5
Range estimate at time 3 (km)	5590.3

Table 11: Example of the outputs from Gooding's algorithm for LEO single-site observations of RSO 15773 [14].

Chapter 4: Results

The results for all scenarios: single- and multi-site observations are displayed in the various tables found in this chapter. The main objectives for this thesis, outlined in Chapter 1.2, form the basis of the analysis discussions found in this chapter as well.

The results displayed in the tables below are the standard deviation and root mean square error (RMSE). These values are calculated using the data points (position, velocity, range) directly from STK as truth data, and the calculated results from Gooding's algorithm output [12][14][36][37][38][39][43]. Bias is the mean error of the results while the standard deviation measures the spread of the error from the mean. The RMSE measures the overall magnitude of error by estimating the distance between the truth values and the results, taking both bias and standard deviation into consideration. The result analysis focuses on the standard deviation and RMSE because they provide a clearer assessment of overall error magnitude and variability between scenarios.

4.1 LEO Results

Simulation Scenario	Position X (km)	Position Y (km)	Position Z (km)	Velocity X (km/s)	Velocity Y (km/s)	Velocity Z (km/s)	Range 1 (km)	Range 2 (km)
Single-site	3.9614	7.3540	4.9131	4.7318×10^{-2}	2.4833×10^{-2}	3.4993×10^{-2}	32.454	31.468
2-site SL	2.5241	6.3472	3.3550	4.2867×10^{-2}	2.2564×10^{-2}	3.3765×10^{-2}	30.016	28.461
SIM 2-site SL	3.4684	3.6797	2.8837	2.2027×10^{-2}	3.1574×10^{-2}	2.3654×10^{-2}	3.0662×10^{-1}	3.6179×10^{-1}
2-site DL	4.8818	7.6099	3.9321	8.2622×10^{-2}	2.6863×10^{-2}	4.7012×10^{-2}	32.536	30.661
SIM 2-site DL	2.6416	3.3106	2.0829	2.3160×10^{-2}	3.0736×10^{-2}	4.4892×10^{-2}	1.5016×10^{-1}	1.5498×10^{-1}
3-site SL	2.5954	6.0460	3.2264	4.8072×10^{-2}	2.4434×10^{-2}	4.0514×10^{-2}	33.829	31.321
SIM 3-site SL	25.727	35.004	48.866	6.6938×10^{-1}	8.8695×10^{-1}	9.6720×10^{-1}	110.47	77.758
3-site DL	4.6104	7.6412	3.7578	8.1360×10^{-2}	3.0061×10^{-2}	5.1253×10^{-2}	36.133	33.653
SIM 3-site DL	5.9917×10^{-1}	6.1403×10^{-1}	5.2861×10^{-1}	1.5618×10^{-3}	3.6922×10^{-3}	2.4478×10^{-3}	1.1150	1.1111

Table 12: The standard deviations of output results from Gooding's algorithm for all nine scenarios for objects in LEO [11][12][13][14][36][37][38][39][43].

Simulation Scenario	Position X (km)	Position Y (km)	Position Z (km)	Velocity X (km/s)	Velocity Y (km/s)	Velocity Z (km/s)	Range 1 (km)	Range 2 (km)
Single-site	3.8282	7.3570	5.3508	4.7598×10^{-2}	2.5446×10^{-2}	3.4551×10^{-2}	33.471	31.386
2-site SL	2.5805	6.0782	3.3982	4.4211×10^{-2}	2.3167×10^{-2}	3.3058×10^{-2}	30.199	28.427
SIM 2-site SL	3.4203	3.5121	3.6351	2.2611×10^{-2}	3.9675×10^{-2}	2.3070×10^{-2}	6.0633	6.1030
2-site DL	4.6331	7.3648	5.7733	7.8425×10^{-2}	4.2801×10^{-2}	6.8775×10^{-2}	59.288	51.085
SIM 2-site DL	2.7236	3.6895	3.8933	2.5544×10^{-2}	2.9076×10^{-2}	4.3824×10^{-2}	5.9922	6.0157
3-site SL	2.4958	5.7908	3.1922	4.8960×10^{-2}	2.4369×10^{-2}	3.8731×10^{-2}	32.886	30.448
SIM 3-site SL	26.216	34.247	51.786	6.6334×10^{-1}	9.0541×10^{-1}	9.6372×10^{-1}	114.00	81.258
3-site DL	4.3899	7.3132	5.7550	7.7209×10^{-2}	4.4144×10^{-2}	6.9924×10^{-2}	59.916	51.143
SIM 3-site DL	6.3901×10^{-1}	6.7561×10^{-1}	5.0238×10^{-1}	1.5724×10^{-3}	3.6556×10^{-3}	2.5781×10^{-3}	1.0590	1.0551

Table 13: The root mean square error of output results from Gooding's algorithm for all nine scenarios for objects in LEO [11][12][13][14][36][37][38][39][43].

Table 12 displays the standard deviation while Table 13 displays the RMSE of the results from using Gooding's algorithm and truth data from STK, specifically for RSOs in LEO [12][14][43]. Green cells means that particular scenario has the lowest values, and thus the best result, within that column. Rows that are gray indicates that specific scenario cannot be represented by the data properly. Meaning that Gooding's algorithm was not able to process the data for some RSOs for that scenario. Reasoning for this is discussed in the following subchapter.

It is clear from both Table 12 and Table 13 that *simultaneous* observations from three host satellites in a diagonal line formation produced the most accurate results for position and velocity vectors of the LEO RSOs compared to all other scenarios. These results far surpass those of two-site observations and, most importantly, single-site observations. It is also apparent that while *simultaneous* observations from two host satellites in a straight line formation produced a better standard deviation for range estimations, the *simultaneous* observations from three host satellites in a diagonal line formation were a very close second. Additionally, the RMSE for the *simultaneous* observations from three host satellites in a diagonal line formation performed better for all values,

including range, when compared to all other scenarios. Since RMSE considers both bias and standard deviation, it is evident that this multi-site scenario has a lower overall magnitude of error and thus outperforms the other scenarios.

It is important to remember that Gooding's algorithm needs two range estimates from the first and third observations times as inputs, so that his algorithm can iteratively refine these range estimates [14]. It is believed that the *simultaneous* observations from two host satellites in a straight line formation obtained slightly better standard deviation for range estimates because the middle and third observation came from the exact same host. Gooding's algorithm requires data, such as host position and LOS units vectors, of the RSO at that time. Which in this case are exactly the same for the second and third observations, thus making this scenario more accurate.

Nonetheless, even with some results being more accurate in either three-site or two-site scenarios, it is evident that multi-site observations produce more accurate observations then single-site observation for RSOs in LEO. Even just taking into consideration the *simultaneous* observations from three host satellites in a diagonal line formation and the single-site observation, this multi-site scenario produced IOD with a decrease in the overall magnitude of error by approximately 88% for position values, 91% for velocity values, and 97% for range values according to Table 13. This was calculated using the **Percent RMSE** equation seen below, where the absolute value of the numerator was taken to ensure that the negative directions from position and velocity values do not effect the overall calculation. To further emphasize the overall difference in IOD accuracy between these two scenarios, Figure 18 displays the RMSE of both scenarios for all results values side by side.

$$\textbf{Percent RMSE} = \left[\frac{|\text{Single-site} - \text{Multi-site}|}{\text{Single-site}}\right] \times 100 \tag{11}$$

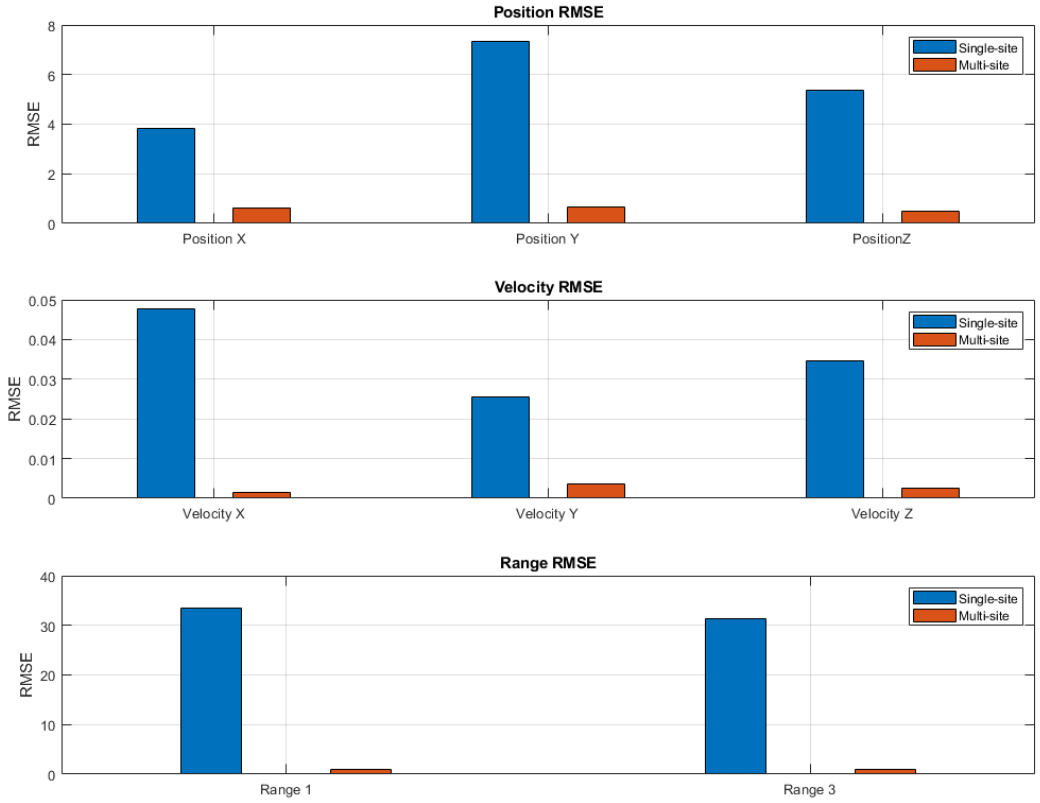

Figure 18: The RMSE comparison between the single-site scenario and the *simultaneous* observations from three host satellites in a diagonal line formation scenario.

It is evident that *simultaneous* observations are beneficial for observing RSO's in LEO. Simultaneous observations allow for a more accurate and straight forward calculation of range, and a greater accuracy in range estimates leads to a greater accuracy in IOD calculations. This is supported by the fact that the *simultaneous* observations from three host satellites in a diagonal line formation produced the most accurate IOD results.

These single-site versus multi-site results further support the ideas in literature that multi-site observation will produce more accurate IOD results for objects in LEO then single-site results. These results are very important because the vast majority of uncategorized objects are in LEO; meaning the multi-site approach will aid with obtaining more accurate orbital data and tracking for

millions of RSOs [1].

4.1.1 LEO Results Analysis

It is evident from the results seen in Table 12 and Table 13, that multi-site observations for objects in LEO produce more accurate IOD than single-site observations. In addition to that, the *simultaneous* three host satellites in a diagonal line formation observations far outperform the *normal* observations for all other scenarios. The overall improvement in IOD accuracy by using multi-site observations supports the ideas seen in literature. As mentioned in Chapter 2.3.6, *simultaneous* multi-site observation have the ability to obtain more straight forward and accurate range measurements than those of single-site. These improved range estimates then help improve overall IOD accuracy as well. It is due to these reasons, which are clearly evident with the LEO results, that the multi-site observations far outperform single-site observations.

From Table 12 and Table 13, the *simultaneous* two host satellites in a diagonal line formation results were not taken into consideration. This is because there was a RSO who's data was not able to be processed through Gooding's algorithm. Upon further inspection of the respective access report, the input data for this specific scenario was not usable for IOD calculations. As mentioned previously, the three observations of the RSO need to form a large enough arc of its orbit in order for the data to be useful in calculating the IOD. The input data for this specific RSO did not form a large enough RSO arc, so the IOD was not able to be calculated. Furthermore, this *simultaneous* two site scenario takes the exact same input data from one host satellite two separate times as seen in the examples from Table 7 and Table 9. This means that because some of the input data is identical, there really is only two different observations of the RSO, instead of the mandatory three different observations. Thus the needed arc in observations, as seen in Figure 19A, was not formed and only a straight line is formed, as seen in Figure 19B. Meaning IOD cannot be calculated. The inability to properly calculate IOD for these scenarios is similar to the common too-short-arc problem in initial orbit determination research [29].

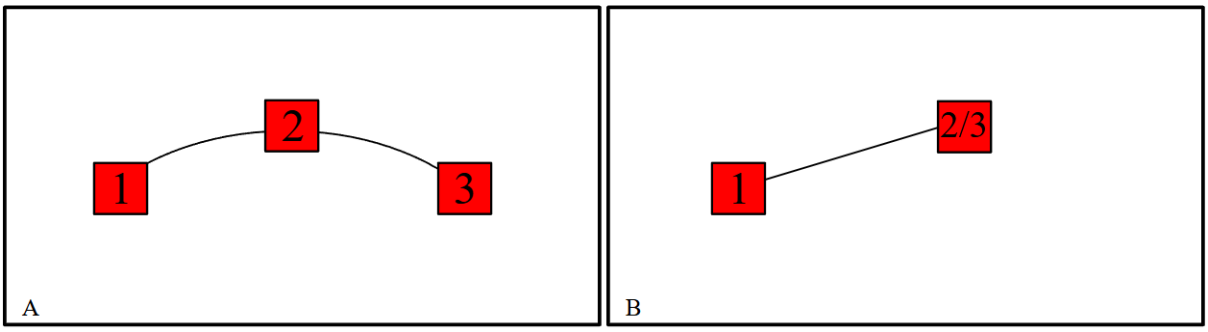

Figure 19: Example of observational arcs. The red boxes represents the RSO being observed at three instances. Image A represents the needed arc of the RSOs orbit which is formed from the three observations. Image B represents the *simultaneous* two host satellite in a diagonal line formation of the RSO who's data was not suitable for IOD calculations.

In regard to diagonal line versus straight line scenarios, neither significantly outperformed the other in all scenarios. While some diagonal line scenarios perform better than their straight line counterparts, the same could be said for the opposite as well. Additionally, there is one simulation scenario which cannot be taken into consideration thus a proper overall comparison is not possible. From these results, the geometry of the constellations does not affect the overall accuracy of IOD calculations of RSOs in LEO.

In addition to constellation geometry, the number of hosts are important to consider as well. There is a two-site scenario that is not suitable for comparison, while all three-site scenarios were. This is because three-site observations allow for a larger range of observability, reducing the chance of a too-short-arc problem. Additionally, simultaneous two-site observations suffer the possibility of not forming an arc in observations, as was the case for the *simultaneous* two host satellites in a diagonal line formation. Due to the larger range of observability, and considering that the *simultaneous* three host satellites in a diagonal line formation produced the most accurate IOD results overall, it is safe to conclude that three-site observation are more reliable than two-site observations.

From the results, it is easy to conclude that multi-site observations of LEO objects generally produce more accurate IODs than those of single-site observations. This further supports the idea

of using multi-site observations rather than single-site observations as seen in the literature.

4.2 MEO Results

Simulation Scenario	Position X (km)	Position Y (km)	Position Z (km)	Velocity X (km/s)	Velocity Y (km/s)	Velocity Z (km/s)	Range 1 (km)	Range 2 (km)
Single-site	1.3003×10^{-1}	8.5073×10^{-2}	1.2641×10^{-1}	6.0563×10^{-5}	9.1300×10^{-5}	1.1958×10^{-4}	3.1313×10^{-1}	2.5280×10^{-1}
2-site (SL)	1.3404×10^{-1}	8.6202×10^{-2}	1.2834×10^{-1}	8.8846×10^{-1}	2.2808×10^{-1}	7.9398×10^{-1}	3.2129×10^{-1}	2.5416×10^{-1}
SIM 2-site (SL)	5.9458	2.5980	3.9005	7.8458×10^{-1}	8.6269×10^{-2}	4.5415×10^{-1}	6.7468	3.3653
2-site (DL)	1.2842×10^{-1}	9.0433×10^{-2}	1.3232×10^{-1}	6.1018×10^{-5}	9.7267×10^{-5}	1.3068×10^{-4}	3.4626×10^{-1}	2.5648×10^{-1}
SIM 2-site (DL)	7.5355	3.6908	3.2673	2.8407	1.3160	4.2393×10^{-1}	3.8402	5.8271
3-site (SL)	1.3436×10^{-1}	8.6903×10^{-2}	1.2922×10^{-1}	$6.2252 \times 10^{5-}$	9.3593×10^{-5}	1.2242×10^{-4}	3.2185×10^{-1}	2.5867×10^{-1}
SIM 3-site (SL)	27.135	7.2349	15.868	6.7130×10^{-4}	4.2869×10^{-3}	2.9429×10^{-3}	31.854	31.867
3-site (DL)	1.2816×10^{-1}	8.5582×10^{-2}	1.2550×10^{-1}	6.1216×10^{-5}	9.1120×10^{-5}	1.1819×10^{-4}	3.1777×10^{-1}	2.4494×10^{-1}
SIM 3-site (DL)	10.385	11.238	27.886	3.7926×10^{-3}	5.0991×10^{-3}	6.3534×10^{-3}	31.906	31.944

Table 14: The standard deviations of output results from Gooding's algorithm for all nine scenarios for objects in MEO [11][12][13][14][36][37][38][39][43].

Simulation Scenario	Position X (km)	Position Y (km)	Position Z (km)	Velocity X (km/s)	Velocity Y (km/s)	Velocity Z (km/s)	Range 1 (km)	Range 2 (km)
Single-site	1.2347×10^{-1}	8.2538×10^{-2}	1.2213×10^{-1}	6.6922×10^{-5}	9.6410×10^{-5}	1.2793×10^{-4}	2.9943×10^{-1}	2.4379×10^{-1}
2-site (SL)	1.2731×10^{-1}	8.3718×10^{-2}	1.2441×10^{-1}	8.8847×10^{-1}	2.2809×10^{-1}	7.9400×10^{-1}	3.0703×10^{-1}	2.4491×10^{-1}
SIM 2-site (SL)	5.6420	3.0477	4.1435	7.8443×10^{-1}	8.5960×10^{-2}	4.5427×10^{-1}	7.4771	7.6348
2-site (DL)	1.2189×10^{-1}	8.9131×10^{-2}	1.2681×10^{-1}	6.7143×10^{-5}	1.0261×10^{-4}	1.3864×10^{-4}	3.3291×10^{-1}	2.4777×10^{-1}
SIM 2-site (DL)	7.5059	4.2284	3.4229	2.8530	1.3363	4.5354×10^{-1}	5.9146	9.2701
3-site (SL)	1.2759×10^{-1}	8.4376×10^{-2}	1.2529×10^{-1}	6.8137×10^{-5}	9.9041×10^{-5}	1.3052×10^{-4}	3.0759×10^{-1}	2.4936×10^{-1}
SIM 3-site (SL)	27.026	7.0669	16.199	7.0788×10^{-4}	4.3791×10^{-3}	2.8411×10^{-3}	32.286	32.299
3-site (DL)	1.2168×10^{-1}	8.3204×10^{-2}	1.2160×10^{-1}	6.7109×10^{-5}	9.6307×10^{-5}	1.2579×10^{-4}	3.0390×10^{-1}	2.3551×10^{-1}
SIM 3-site (DL)	10.122	11.780	28.888	3.8469×10^{-3}	4.8376×10^{-3}	6.4302×10^{-3}	32.778	32.819

Table 15: The root mean square error of output results from Gooding's algorithm for all nine scenarios for objects in MEO [11][12][13][14][36][37][38][39][43].

Table 14 displays the standard deviation and Table 15 displays the RMSE of the results from using Gooding's algorithm and truth data from STK , specifically for RSOs in MEO [12][14][43]. Green cells means that particular scenario had the smallest values, and thus the best result, within that column.

The *normal* observations from three host satellites in a diagonal line formation produced the most accurate results for majority of position, velocity and range elements. While five elements performed better in this scenario, the remaining three elements performed better in single-site scenario. It is important to note however, that even though three elements performed slightly better in the single-site scenario, the three host satellites in a diagonal line formation produced values similar to those of single-site.

Just taking into consideration the *normal* observation from three host satellites in a diagonal line formation and the single-site observation, this multi-site scenario produced IOD with a decrease in the overall magnitude of error by approximately 0.90% for position values, 0.69% for velocity values, and 2.4% for range values according to Table 15. This was calculated using the **Percent**

RMSE equation seen in Chapter 4.1. Although noise is not considered in this analysis, these results may be below the noise floor. However, the overall trend in the results is visible and still support the use of multi-site observations. These results show that the three host satellites in a diagonal line formation produced accurate results overall for MEO objects and support the idea that multi-site observation can produce more accurate IOD results then single-site observations. To further emphasize the overall difference in IOD accuracy between these two scenarios, Figure 20 displays the RMSE of both scenarios for all results values side by side.

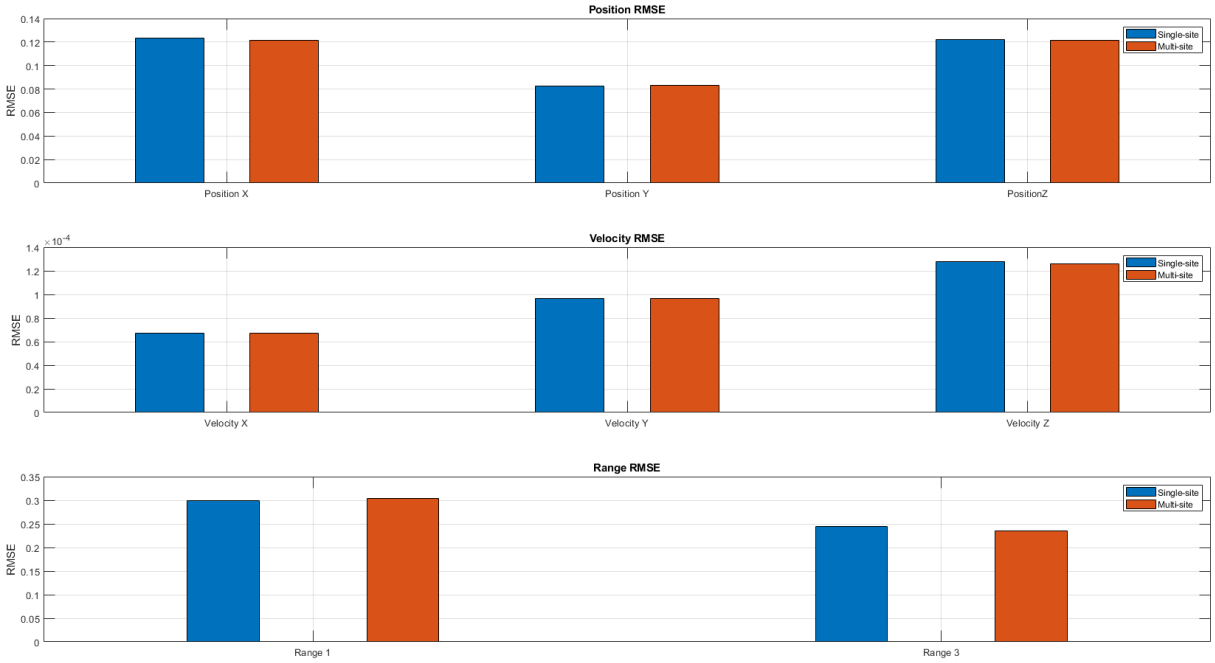

Figure 20: The RMSE comparison between the single-site scenario and the *normal* observation from three host satellites in a diagonal line formation scenario.

It is also important to point out that even though the observations from the host satellites in a diagonal line formation produced some accurate results, these observations were not done simultaneously. In fact looking at Table 15, *simultaneous* observations for two or three sites produce larger RMSE then any scenario with *normal* observations. This is due to the fact that all host satellites are in LEO while the RSOs are in MEO, meaning they are significantly further away from each other. Because of this, *simultaneous* observations produce much shorter observational

arc's thus making it difficult to produce accurate results.

Nonetheless, even with some results being more accurate in different scenarios, it is evident that multi-site observations produces slightly more accurate IOD then single-site observation for RSOs in MEO and are still worth the effort to pursue. These results further support the ideas in literature that multi-site observations will produce more accurate IOD for objects in MEO than single-site results.

4.2.1 MEO Results Analysis

By analyzing the IOD results for MEO objects, it is evident that multi-site observations, specifically *normal* observations for three host satellites in a diagonal line formation, outperform the single-site observations. As mentioned in Chapter 2.3.6, multi-site scenarios have the ability to obtain a larger range of observability, which decreases the possibility of having too short of an arc for IOD calculations. This is one reason that the three host satellites in a diagonal line formation for *normal* observations performed better overall than the single-site scenario. However, this point is also the reason why the *simultaneous* observation for MEO RSOs did not perform well; the arcs for the observations where too small.

In regard to diagonal line versus straight line scenarios, neither fully outperformed the other. While some diagonal line scenarios perform better than they straight line counterparts, the same could be said for the opposite as well. From these results, the geometry of the constellations does not affect the overall accuracy of IOD calculations of MEO objects.

Additionally, there are no scenarios in which Gooding's algorithm was not able to process the data from any of the MEO RSOs. This means that for every scenario, with either two or three hosts, the observational input data formed a large enough arc that was suitable for IOD calculations. With that said, three-site observations are still favoured over two-site observations because they allow for larger range of observability, resulting in a reduced chance of a too-short-arc problem.

From the results, multi-site observations of MEO objects produce more accurate IODs than those of single-site observations nonetheless. This further supports the idea of using multi-site

observations rather than single-site observations as seen in the literature.

4.3 GEO Results

Simulation Scenario	Position X (km)	Position Y (km)	Position Z (km)	Velocity X (km/s)	Velocity Y (km/s)	Velocity Z (km/s)	Range 1 (km)	Range 2 (km)
Single-site	8.1074	1.9749	6.0850×10^{-1}	3.6373×10^{-3}	2.1543×10^{-3}	9.1318×10^{-4}	14.371	4.4030
2-site (SL)	8.2749	1.9596	5.7366×10^{-1}	3.5743×10^{-3}	2.2322×10^{-3}	9.527×10^{-4}	14.635	4.8364
SIM 2-site (SL)	5.0690	2.9386	5.9042×10^{-1}	2.3110×10^{-2}	1.3812×10^{-2}	3.9909×10^{-3}	5.1264×10^{-1}	5.2175×10^{-1}
2-site (DL)	16.541	3.0334	7.6150×10^{-1}	7.3535×10^{-3}	3.5073×10^{-3}	1.8586×10^{-3}	26.922	9.2433
SIM 2-site (DL)	4.9152	3.5715	6.1019×10^{-1}	7.3977×10^{-2}	1.1161×10^{-1}	2.0411×10^{-2}	8.5797×10^{-1}	3.6070×10^{-1}
3-site (SL)	8.4365	1.9886	5.7937×10^{-1}	3.5997×10^{-3}	2.2473×10^{-3}	9.6419×10^{-4}	14.835	4.9412
SIM 3-site (SL)	93.599	5.5301	1.9478	2.0705×10^{-3}	8.7237×10^{-3}	1.8790×10^{-3}	96.092	96.095
3-site (DL)	16.645	3.0489	7.6507×10^{-1}	7.3680×10^{-3}	3.5158×10^{-3}	1.8664×10^{-3}	27.053	9.3040
SIM 3-site (DL)	6.1184	7.9940	1.5476	3.7646×10^{-2}	1.1972×10^{-2}	4.3157×10^{-3}	9.6530	9.6652

Table 16: The standard deviations of output results from Gooding's algorithm for all nine scenarios for objects in GEO [11][12][13][14][36][37][38][39][43].

Simulation Scenario	Position X (km)	Position Y (km)	Position Z (km)	Velocity X (km/s)	Velocity Y (km/s)	Velocity Z (km/s)	Range 1 (km)	Range 2 (km)
Single-site	9.0397	1.8773	6.8803×10^{-1}	4.2076×10^{-3}	2.1580×10^{-3}	1.0525×10^{-3}	14.439	5.1548
2-site (SL)	9.1804	1.8646	6.4118×10^{-1}	4.1480×10^{-3}	2.2376×10^{-3}	1.0933×10^{-3}	14.721	5.6132
SIM 2-site (SL)	4.9544	2.9027	5.7500×10^{-1}	2.3095×10^{-2}	1.3889×10^{-2}	4.0752×10^{-3}	5.9100	5.7709
2-site (DL)	16.040	3.0108	7.2353×10^{-1}	7.3189×10^{-3}	3.6165×10^{-3}	1.8126×10^{-3}	25.774	9.2196
SIM 2-site (DL)	4.6048	3.5566	5.7624×10^{-1}	7.7709×10^{-2}	1.0567×10^{-1}	1.9789×10^{-2}	5.7797	5.8469
3-site (SL)	9.3485	1.8915	6.4789×10^{-1}	4.1719×10^{-3}	2.2547×10^{-3}	1.1049×10^{-3}	14.923	5.7293
SIM 3-site (SL)	94.733	6.2180	1.8985	1.9666×10^{-3}	8.6616×10^{-3}	1.9350×10^{-3}	94.954	94.958
3-site (DL)	16.143	3.0275	7.2700×10^{-1}	7.3345×10^{-3}	3.6259×10^{-3}	1.8203×10^{-3}	25.901	9.2810
SIM 3-site (DL)	5.8045	8.0543	1.5061	3.7792×10^{-2}	1.2137×10^{-2}	4.2285×10^{-3}	10.044	10.037

Table 17: The root mean square error of output results from Gooding's algorithm for all nine scenarios for objects in GEO [11][12][13][14][36][37][38][39][43].

Table 16 displays the standard deviation and Table 17 displays the RMSE of the results from using Gooding's algorithm and truth data from STK, specifically for RSOs in GEO [12][14][43]. Green cells means that particular scenario had the smallest value, and thus the best result, within that column. Rows that are gray means that specific scenario cannot be represented by the data properly. Meaning that Gooding's algorithm was not able to process the data for some RSOs for that scenario. Reasoning for this will be discussed in the following subchapter.

The results in Table 16 and Table 17 are by far the most difficult to decipher since there is no clear or evident pattern in the results. While the table shows that some velocity and range measurements are more accurate in single-site scenarios, the rest of the results are more accurate in a variety of multi-site scenarios. Additionally, since not one specific multi-site scenario performed better than the others, the overall improvement in IOD accuracy is not clear. However, for the sake of comparison, just taking into consideration the *simultaneous* observations from three host satellites in a diagonal line formation and the single-site observation, the single-site scenario overall produced a decrease in the overall magnitude of error by approximately 62% for position values,

82% for velocity values, and 46% for range values according to Table 17. Meaning that the single-site observations performed better than the *simultaneous* observations from three host satellites in a diagonal line formation. This was calculated using the equation below for **Single-site Percent RMSE**, which is similar to the equation in Chapter 4.1. To further emphasize the overall difference in IOD accuracy between these two scenarios, Figure 21 displays the RMSE of both scenarios for all results values side by side.

$$\textbf{Single-site Percent RMSE} = \left[\frac{|\text{Multi-site} - \text{Single-site}|}{\text{Multi-site}}\right] \times 100 \tag{12}$$

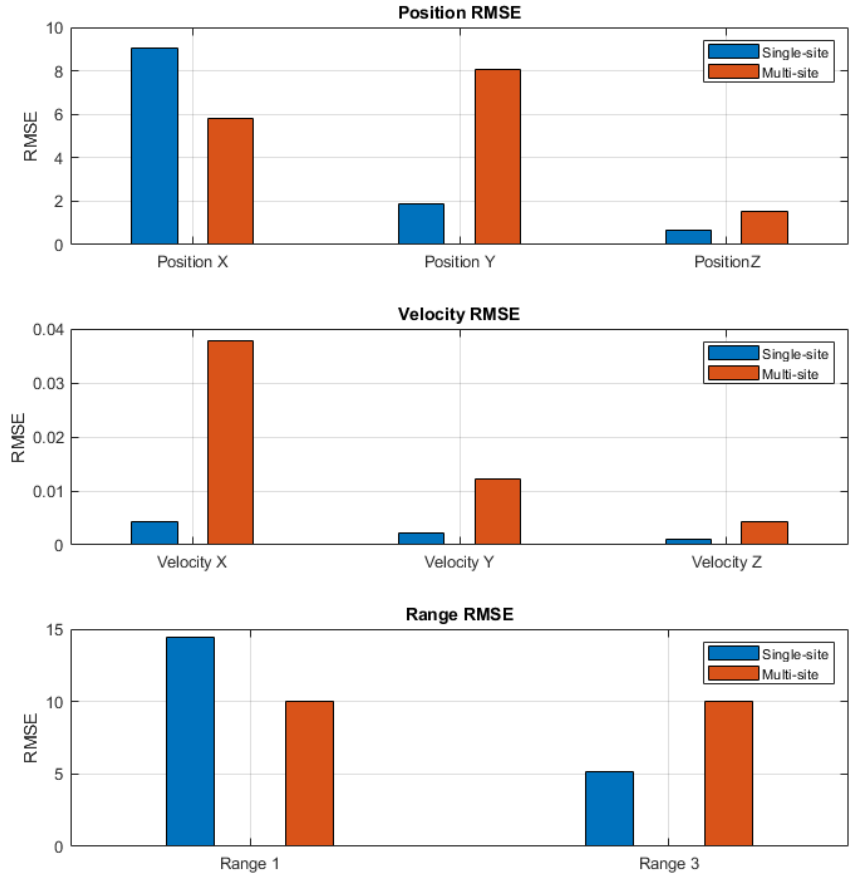

Figure 21: The RMSE comparison between the single-site scenario and the *simultaneous* observations from three host satellites in a diagonal line formation scenario.

As seen in Table 17, *simultaneous* observations for two or three sites produce larger RMSE then any scenario with *normal* observations. This again has to do to the fact that *simultaneous* observation of GEO objects, from LEO hosts, can struggle to provide a large enough arc in observations for accurate IOD calculations. It is due to these reasons that while multi-site observations are worth the effort to use for GEO RSO observations, these observations are better done *normally* rather than *simultaneously*.

It is evident that five elements perform better in multi-site scenarios, even if one specific scenario does not stand out, and the remaining three elements performed better in single-site scenarios. Although the comparison between the single-site scenario and the *simultaneous* three-site diagonal line formation favoured the single-site scenario, the overall trend in the data indicate that the multi-site scenarios, when considered collectively, produced lower RMSE than the single-site scenario. Giving the conclusion that multi-site observations generally performed better than single-site observations. Even with the results not being as straightforward as those for LEO objects, it is still worth the effort to use multi-site observations. These results further support the ideas in literature that multi-site observations will improve IOD accuracy for objects in GEO.

4.3.1 GEO Results Analysis

Although deciphering which specific scenario produced the most accurate IOD results for GEO objects is not straightforward, it is still evident that multi-site observations overall could be more beneficial than single-site observations. As mentioned in Chapter 2.3.6, multi-site observations have a larger range of observability, reducing the possibility of having too short of an arc for IOD calculations. This is an extremely important aspect when observing objects in GEO. GEO RSOs are farther in distance and typically slower in speed, meaning that observing them from other orbits, such as LEO, poses a risk of having a too-short-arc. By having multiple observers, the observation time, and thus observational arc, would increase; allowing for more accurate IOD calculations. Furthermore, the range for a RSO is more easily calculated when using multiple observers, which also improves overall IOD accuracy.

From Table 16 and Table 17, both *simultaneous* two-site observational scenarios results were not taken into consideration. This is because there was at least one RSO who's data was not able to be processed through Gooding's algorithm. Upon further inspection of the respective access reports, the input data for these specific RSOs were not usable for IOD calculations. This is because the three mandatory observations of a RSO needs to form a large enough arc of its orbit in order for the data to be useful in calculating IODs. The input data for these specific GEO RSOs did not form large enough RSO arcs, so IODs were not properly calculated. A visual representation of this is seen in Figure 4. Furthermore, the *simultaneous* two-site scenarios take the exact same input data from one host satellite two separate times as seen in the examples from Table 7 and Table 9. This means that because some input data is identical, there really is only two different observations of the RSO, instead of the mandatory three different observations. Meaning an arc is not formed at all. This is identical to the grey line scenario seen for the LEO results, where a visual representation of this issue is seen in Figure 19. The inability to properly calculate IOD for these scenarios is similar to the common too-short-arc issue in initial orbit determination research [29].

In regards to diagonal line versus straight line scenarios, neither completely outperformed the other. While some diagonal line scenarios perform better than they straight line counterparts, it could be said the same for the opposite as well. Additionally, there are two simulation scenarios in which cannot be taken into consideration thus a proper comparison is not possible. From these results, the geometry of the constellations does not affect the overall accuracy of IOD calculations for GEO RSOs.

In addition to constellation geometry, the number of hosts are important to consider as well when analyzing the results. There are two two-site scenarios that are not suitable for comparison, while all three-site scenarios were. This is because three-site observations allow for a larger range of observability, reducing the chance of a too-short-arc problem. Due to this larger range of observability, it is safe to conclude that three-site observation are more reliable than two-site observations for RSOs in GEO.

From the results, multi-site observations of GEO objects can produce more accurate IODs

overall than those of single-site observations nonetheless. This further supports the idea of using multi-site observations rather than single-site observations for objects in GEO, as seen in the literature.

4.4 Overall Result Analysis

Although it is quiet evident as too which simulation scenario performed the best overall for LEO objects, MEO and GEO objects were a bit harder to decipher. To generalize the overall analysis of MEO and GEO RSOs one can conclude that as the RSOs orbit gets further out, it becomes increasingly more difficult to decipher which specific scenario produced the best IOD results. This lack of consistency is due to the decrease in the observation arc size. As the RSOs get further away from the host, the possibility of a too-short-arc for IOD calculations increases.

Additionally for all orbits, it is evident that for multi-site observations overall, three-site observations are a more reliable process than two-site observations. This is supported by the fact that numerous two-site scenarios (grey lines) were not considered in the analysis due to the reasons stated in their respective Chapters. Additionally, three-site observations allow for a larger range of observability, reducing the chance of a too-short-arc problem. Furthermore, when considering only the best results (green cells), the three-site observations performed better than the two-site observations as a whole for all orbits. Another important point is that *simultaneous* multi-site observations performed better than *normal* multi-site observations for objects in LEO. However, for MEO and GEO objects, *normal* multi-site observations are possibly the more reliable way to go when taking into consideration observational arc size. Lastly, it is evident that for multi-site observations overall, neither the diagonal line or straight line scenario outperformed the other; leading to the understanding that the geometry of the constellations did not affect the overall accuracy of IOD calculations.

There are a variety of reasons as to why the RMSEs are not zero when using simulated data. Although STK is a reliable simulation software, there is no such thing as perfect error free data, simulated or not [12]. One example of this is seen with the *simultaneous* observational

data. The *simultaneous* observations for all observers could only happen when all hosts FOVs overlapped which would cause time constraints. However, it could be seen as beneficial that these near *simultaneous* times were not always done with an exactly zero second time difference, since absolute *simultaneous* observations are also highly difficult to achieve with real data.

Another reason for a none-zero RMSE is due to the IOD algorithm. Although Gooding's algorithm is one of the most reliable and robust IOD algorithm within literature, it is not absolutely perfect due to mathematical and logical restraints. Since the simulated data from STK is processed through Gooding's algorithm, other errors could arise. One example of this is that his algorithm performs better when range estimates are more accurate, even though his algorithm iteratively refines these estimates [14][46]. Nonetheless, his IOD is still one of the most robust in the literature.

An important aspect of this research, is that although simulated data was used, the overall process can be repeated with real data. In real IOD settings, the quality of the data highly influences the quality of the results. The host orbital elements, specifically its position vectors, must be extremely accurate not only because it is directly used in the IOD algorithm, but because it is also used for range and LOS unit vector calculations. Meaning that any errors from the hosts GPS and attitude technology will propagate through the IOD calculations and decrease its overall accuracy. Because of this, the performance quality of the star tracker onboard the host is extremely important. In regards to real multi-site *simultaneous* observations, there will be constraints to how *simultaneous* the observations can be. These constraints could stem from limitations in technology or even inaccuracies in the multiple FOVs not properly lining up. With that said, real data can be used through the same process as described in this thesis, however the overall quality of the data will highly influence the overall accuracy of the IOD results.

Chapter 5: Conclusion

5.1 Overview of Thesis

Continued contributions to SSA research remain crucial in mitigating RSO congestion and collisions within Earths various orbits. A focal point for these efforts is using initial orbit determination to obtain orbital data on millions of RSOs. While single-site observations are currently the most common form of observations for IOD, the results of these observations lack the accuracy needed for SSA objectives. It is because of this demand for improved orbital accuracy that this thesis focuses on not only improving accuracy for IOD calculations, but also supporting the foundation for various other strands of orbital research.

The ability to observe and study RSOs through space-based observations without adding to RSO congestion is the ideal scenario for SSA. This thesis supported the ideas found within the literature stating that active star-trackers can be used for dual purposes; attitude determination and RSO observations. Since there are thousands of star-trackers currently orbiting Earth, the possibility of observing RSOs in various orbits is high, and multi-site observations are possible. As described in Chapter 3, the FAI star-tracker was used for both the single- and multi-site scenarios. Furthermore, Chapter 2.3.7, fully breaks down the steps for obtaining the necessary IOD input values from star-tracker images. The results from these scenarios are promising and it can be confidently stated that real star-tracker images could be used for RSO IOD calculations.

The main effort towards SSA contribution in this thesis was to prove that multi-site observations produce better IOD accuracy overall compared to single-site observations. As outlined in Chapter 3, these simulations provided the data needed to test a variety of scenarios for single- and multi-site observations of RSOs in three different orbits; LEO, MEO, and GEO. By comparing the results from a singular host, double hosts, and triple hosts, it was evident that using multiple hosts increased overall IOD accuracy. Additionally, these observations were taken of RSO from three different orbits, to determine how the distance between the host(s) and RSO(s) effected the overall IOD accuracy. These orbital differences allowed for a more in depth accuracy analysis which aided in

determining how beneficial multi-site observation would be for RSOs in different orbits. Lastly, the multi-site observations were taken from two different constellation geometries. Where the results formed a baseline for future work for formation flying with the aim for IOD observations specifically.

While the results from this thesis were obtained through simulated data, all of the orbital data used to simulate the hosts and RSOs were from real data sources. The overall data processes and calculations were also intentional to guarantee that the same steps could be followed once real data was acquired.

5.2 Contributions

The contributions of this work starts with its continuous support in using star-trackers for RSO observations. It is evident within the literature that star-trackers can be used to observe RSOs [7][8][9][10]. This thesis takes it a step further by demonstrating that these observations provide the necessary input information needed for calculating IOD. A major goal in SSA research is improving the range estimates of RSOs and, as described in Chapter 2.3.7, the pixel location of the RSO can be used to calculate its LOS unit vectors and estimate the range between the host and RSO. This chapter also demonstrates that using star-tracker images from multiple hosts is a more efficient way in estimating the RSOs range. Multiple star-trackers allow for simultaneous observations of the RSO which removes the need to account for change in position over time. This allows for a much simpler and straight forward range calculation. Due to this analysis, it is evident that using star-tracker images, specifically from multiple hosts, is beneficial for RSO observations and IOD calculations. Additionally, even though simulated data was used, the overall processes described throughout this work can also be used for real data.

In the course of this work, IOD accuracy from multi-site observations are studied from a variety of scenarios and compared to that of single-site observations. A main objective of SSA research is improving IOD accuracy to help with RSO congestion and collision predictions; and this thesis proves that multi-site observations does that. Within literature, multi-site observations are not extensively studied, and much of the research that has been done had used two observation sites

[9][32][34][35]. This thesis tested observations done by a singular host, double host, and triple hosts. As described in Chapter 3, there are nine scenarios in which RSO were observed. For a number of these scenarios, the multi-site observations that were done with three hosts satellites produced IOD results with greater accuracy then results from both a single host and two hosts. Additionally, having three hosts, rather then one or two, allow for a larger range of observability; reducing the chance of a too-short-arc problem arising. Furthermore, using more than three host satellites is redundant for the objectives of this thesis since, for Gooding's IOD algorithm, only three observations in total can be used. Therefore, this thesis concludes that three host satellites is the ideal amount of space-based observers, for the objectives of this research, since they improve IOD accuracy overall and provide a larger range of observability. This discovery is beneficial when deciding on the amount of observers to use for SSA research involving IOD.

Another main objective for this multi-site research, was determining how the accuracy from all nine scenarios change when observing RSOs in different orbits. Within the sparse literature found on multi-site observations, the number of RSOs studied were limited, not real, or all from similar orbits [9][32][34][35]. This thesis takes multi-site observations a step forward and tests a larger amount of RSOs for all nine scenarios for objects in LEO, MEO and GEO using TLE data. The number of RSOs and orbits considered provided a more comprehensive analysis that extended beyond the scope of the previous literature. Moreover, multi-site observations allow for simultaneous observation of RSOs. As discussed in Chapter 4, IOD for objects in LEO benefit from *simultaneous* multi-site observations, while objects in MEO and GEO benefit more for *normal* multi-site observations. While Chapter 4 goes into great detail for each scenario and each orbit, it can be said that the IOD accuracy is affected by the distance between the host(s) and RSO. This is due to the fact that as the distance between the host(s) and RSO increases, the observational arc becomes shorter; especially when using simultaneous observations. This too-short-arc problem is one common challenge in SSA orbital research. Nevertheless, the overall results demonstrate that using multi-site observations generally produce more accurate results than single-site observations. Furthermore, multi-site *simultaneous* observations still allow for simpler range estimates than single-

site observations. These results are beneficial for SSA research since it confirms that multi-site observations, specifically from star-trackers located in LEO, still produce better IOD accuracy then single-site observations for RSOs in many different orbits.

Lastly, this research creates a foundation in constellation research for IOD purposes. As described in Chapter 3, the scenarios created for multi-site observations were done using a straight line constellation and a diagonal line constellation. When comparing the results between the two geometries, neither scenarios outperformed the other. Since neither formation produce more accurate results, this suggests that constellation geometry has little effect on overall IOD accuracy. This would be an ideal outcome, as it supports the use of existing star trackers, since their relative orientations would not greatly effect IOD results. Even though these are only two out of the many different constellations possible, it is a good foundation for constellation flying IOD research. Although formation flying is out of the scope of this research, these results can be the connection between IOD research and constellation flying research.

To conclude, it is evident that overall multi-site observations truly do produce more accurate IOD for a variety of scenarios when compared to single-site observations. These results are crucial for SSA research since improvement in IOD accuracy is beneficial for combating RSO congestion and collision possibilities. While the overall IOD accuracy improvement varied for the different orbits, all IOD results benefit from the use of multi-site observations regardless of the orbit. Furthermore, the results of this research are beneficial since space-based observations are obtainable by the already orbiting star-trackers, and will not add to the RSO congestion in Earths orbits. With that said, it is beneficial to push for multi-site observations in order to improve IOD accuracy overall and to contribute to major SSA objectives.

5.3 Future Work

Research on enhancing techniques for SSA is an ongoing effort, especially in the field of orbit determination. The findings of this research serve an important role in supporting the advancements in future projects. The use of star-trackers for RSO observations is beneficial for bringing more use

to common technologies and expanding its use further by merging it into IOD research specifically. The results obtained provide evidence that multi-site observations improve IOD accuracy and can be useful for obtaining IOD on RSOs in LEO, MEO, and GEO. Furthermore, the multi-site constellation formations provide a strong foundation for future constellation projects with IOD objectives in mind. The overall goal of this work is to provide evidence and new insights of RSO observations for IOD, and to foster further development in orbital strategies for SSA endeavors.

The simulations conducted in this research were generated using ephemeris and TLE data to provide a realistic foundation for all the simulation scenarios. However, no additional measurement noise was included into the scenarios, making both the simulations and the resulting data deterministic. The first step for future work is to introduce noise into the simulations and use the resulting observational data for IOD calculations. Since the next major phase of this research involves using real data, investigating the effects of measurement noise on both the simulations and resulting IOD will provide valuable information on the sensitivity of this research approach. Furthermore, this analysis will help identify any potential limitations when using real optical data.

The data for this thesis is obtained through simulations, since there is no real public multi-site data available. The next major step for future research is to perform this multi-site analysis with real data instead. Although the steps for this thesis are centered around simulated data, the overall process is designed with real data in mind. The process of obtaining the input data needed for IOD calculations from real star-tracker images is outlined in Chapter 2.3.7. The data obtained from star-tracker(s) can then be used directly into Gooding's algorithm and processed to obtain IOD. While real public star-tracker data is available for a single site, the next phase would also need to test real data from multiple star-trackers.

This thesis built off of research done on star-trackers which focuses on LEO observations. Due to this, and the fact that most satellites (and thus star-trackers) are located in LEO, all the host satellites are simulated in LEO as described in Chapter 3. When calculating IOD from optical observations, a common issue found in orbital research is having a too short-arc of the RSO. This means that the observations did not form a large enough arc to accurately calculate IOD. As seen in

this research, this can happen when the host(s) and RSO are in different orbits and thus separated by a large distance. To combat this, future work should involve testing the multi-site observations of RSOs in multiple orbits, while having the host located in MEO and GEO orbits instead. This could further test and refine multi-site observations possibilities and see if IOD accuracy could be improved even further.

Lastly, this thesis builds a strong foundation for constellation research focused on IOD purposes. As outlined throughout this thesis, two different constellation formations were tested. Since the results between these two constellation suggested that the geometry does not affect the accuracy of IOD, it would be interesting to test more complex constellations and compare results. Future work can be done on testing a larger variety of constellations geometry types and determine if any produce better IOD accuracy from their observations. While formation flying is beyond the scope of this research, the overall results provide a strong foundation for expanding and blending the two research areas together.

With that said, the overall goal of this thesis was to support SSA advancements in orbital research. From the results and overall analysis, it is safe to conclude that multi-site observations improve IOD accuracy and should be the next major step for future SSA research.

References

[1] European Space Agency, "Space environment statistics," Apr. 2026. [Online]. Available: https://sdup.esoc.esa.int/discosweb/statistics/

[2] R. Qashoa and R. Lee, "Classification of Low Earth Orbit (LEO) Resident Space Objects' (RSO) Light Curves Using a Support Vector Machine (SVM) and Long Short-Term Memory (LSTM)," *Sensors*, vol. 23, no. 14, Jul. 2023.

[3] J. A. Kennewell and B.-N. Vo, "An overview of space situational awareness," in *Proceedings of the 16th International Conference on Information Fusion*, Jul. 2013, pp. 1029–1036.

[4] D. L. Oltrogge and S. Alfano, "The technical challenges of better Space Situational Awareness and Space Traffic Management," *Journal of Space Safety Engineering*, vol. 6, no. 2, pp. 72–79, Jun. 2019.

[5] D. A. Vallado, *Fundamentals of Astrodynamics and Applications*, 4th ed. Hawthorne, CA: Microcosm Press, 2013.

[6] A. Porras-Hermoso, R. Qashoa, R. S. K. Lee, J. Cubas, and S. Pindado, "On the space observation of resident space objects (rsos) in low earth orbits (leos)," *Remote Sensing*, vol. 17, no. 16, 2025. [Online]. Available: https://www.mdpi.com/2072-4292/17/16/2844

[7] S. Dave, R. Clark, and R. S. K. Lee, "RSOnet: An Image-Processing Framework for a Dual-Purpose Star Tracker as an Opportunistic Space Surveillance Sensor," *Sensors*, vol. 22, no. 15, Jul. 2022.

[8] R. Clark, Y. Fu, S. Dave, and R. Lee, "Simulation of RSO Images for Space Situation Awareness (SSA) Using Parallel Processing," *Sensors*, vol. 21, no. 23, Nov. 2021.

[9] M. Liu, H. Wang, H. Yi, Y. Xue, D. Wen, F. Wang, Y. Shen, and Y. Pan, "Space Debris Detection and Positioning Technology Based on Multiple Star Trackers," *Applied Sciences*, vol. 12, no. 7, Mar. 2022.

[10] P. Kunalakantha, A. V. Baires, S. Dave, R. Clark, G. Chianelli, and R. S. K. Lee, "Stratospheric Night Sky Imaging Payload for Space Situational Awareness (SSA)," *Sensors*, vol. 23, no. 14, Jul. 2023.

[11] University of Calgary. (2013) Welcome to e-pop. [Online]. Available: https://epop.phys.ucalgary.ca/

[12] Ansys, Inc. Systems Tool Kit STK. Ansys. [Online]. Available: https://www.ansys.com/products/missions/ansys-stk

[13] University of Calgary. (2013, Sep.) Fast Auroral Imager FAI. [Online]. Available: https://epop.phys.ucalgary.ca/fai/

[14] R. H. Gooding, "A New Procedure for Orbit Determination Based on Three Lines of Sight (Angles Only)," Defence Research Agency, Tech. Rep., Apr. 1993.

[15] European Space Agency. (2026) About Space Debris. [Online]. Available: https://www.esa.int/Space_Safety/Space_Debris/About_space_debris

[16] United States Space Force. Basic Description of the Two Line Element (TLE) Format. Space-Track.org. [Online]. Available: https://www.space-track.org/documentation#/tle

[17] Spire Global. Two-Line Elements (TLE). [Online]. Available: https://spire.com/spirepedia/two-line-elements-tle/

[18] Kaitlyn. (2020) Two-Line Elements (TLE). [Online]. Available: https://kaitlyn.guru/projects/two-line-elements-tle/

[19] V. Suthakar, A. A. Sanvido, R. Qashoa, and R. S. K. Lee, "Comparative Analysis of Resident Space Object (RSO) Detection Methods," *Sensors*, vol. 23, no. 24, Dec. 2023.

[20] S. Kazemi, N. L. Azad, K. A. Scott, H. B. Oqab, and G. B. Dietrich, "Orbit determination for space situational awareness: A survey," *Acta Astronautica*, vol. 222, pp. 272–295, Sep. 2024.

[21] S. Clemens, "ON-ORBIT RESIDENT SPACE OBJECT (RSO) DETECTION USING COMMERCIAL GRADE STAR TRACKERS," May 2019.

[22] S. Dave, R. Clark, G. Chianelli, and R. Lee, "Machine learning implementation for in-orbit RSO orbit estimation using star tracker cameras," 2020.

[23] V. Suthakar, P. Kunalakantha, R. S. Lee, G. Sohn, and N. R. Laboratory, "DUST : An On-Orbit Start-Tracker Benchmark for RSO Detection and Attitude Estimation," Dec. 2025.

[24] Y. Jeong, V. Suthakar, R. Qashoa, G. Sohn, and R. S. K. Lee, "OrbitTrack: Advanced RSO detection and tracking from wide field-of-view on-orbit images," *Advances in Space Research*, vol. 76, no. 8, pp. 4387–4400, Oct. 2025.

[25] V. Suthakar, I. Porto, M. Myhre, A. A. Sanvido, R. Clark, and R. S. K. Lee, "RSONAR: Data-Driven Evaluation of Dual-Use Star Tracker for Stratospheric Space Situational Awareness (SSA)," *Sensors*, vol. 26, no. 1, Dec. 2025.

[26] R. Qashoa, V. Suthakar, G. Chianelli, P. Kunalakantha, and R. S. K. Lee, "Technology Demonstration of Space Situational Awareness (SSA) Mission on Stratospheric Balloon Platform," *Remote Sensing*, vol. 16, no. 5, Feb. 2024.

[27] S. Dikmen, "Development of Star Tracker Attitude and Position Determination System for Spacecraft Maneuvering and Docking Facility," https://documentcloud.adobe.com/spodintegration/index.html#, 2016.

[28] A. V. Baires, "IMAGE CLASSIFICATION AND INITIAL ORBIT DETERMINATION OF RESIDENT SPACE OBJECTS (RSO)," Jan. 2024.

[29] Y. Geng, E. Bai, F. Wu, Z. Zhao, and M. Sun, "Initial orbit determination for too-short-arc targets from space-based observations via a normal vector method," *Aerospace Science and Technology*, vol. 176, p. 112073, Sep. 2026.

[30] Z. Zhang, G. Zhang, J. Cao, C. Li, W. Chen, X. Ning, and Z. Wang, "Overview on Space-Based Optical Orbit Determination Method Employed for Space Situational Awareness: From Theory to Application," *Photonics*, vol. 11, no. 7, Jun. 2024.

[31] M. R. Ackermann, C. R. R. Kiziah, P. C. Zimmer, John T McGraw, and David D. Cox, "A SYSTEMATIC EXAMINATION OF GROUND-BASED AND SPACE-BASED APPROACHES TO OPTICAL DETECTION AND TRACKING OF SATELLITES," Apr. 2015.

[32] J. Choi, Y.-J. Choi, H.-S. Yim, J. Jo, and W. Han, "Two-Site Optical Observation and Initial Orbit Determination for Geostationary Earth Orbit Satellites," *Journal of Astronomy and Space Sciences*, vol. 27, pp. 337–343, Dec. 2010.

[33] L. George, *Introduction to Orbital Mechanics*. [Online]. Available: https://colorado.pressbooks.pub/introorbitalmechanics/

[34] M. Porfilio, F. Piergentili, and F. Graziani, "Two-site orbit determination: The 2003 GEO observation campaign from Collepardo and Mallorca," *Advances in Space Research*, vol. 38, no. 9, pp. 2084–2092, Jan. 2006.

[35] T. I. Burroni, S. Husain, P. Servidia, K. Thangavel, and R. Sabatini, "Constellation of Formations for Autonomous Resident Space Object Detection Using Star Trackers," Oct. 2024.

[36] A. W. Odell and R. H. Gooding, "Procedures for solving Kepler's equation," *Celestial Mechanics*, vol. 38, no. 4, pp. 307–334, Jan. 1986.

[37] R. H. Gooding, "On universal elements, and conversion procedures to and from position and velocity," *Celestial Mechanics*, vol. 44, no. 3, pp. 283–298, Oct. 1988.

[38] ——, “A procedure for the solution of Lambert’s orbital boundary-value problem,” *Celestial Mechanics and Dynamical Astronomy*, vol. 48, no. 2, pp. 145–165, Jan. 1990.

[39] ——, “A new procedure for the solution of the classical problem of minimal orbit determination from three lines of sight,” *CELESTIAL MECHANICS AND DYNAMICAL ASTRONOMY*, vol. 66, no. 4, pp. 387–423, Dec. 1996.

[40] T. A. Henderson, D. Mortari, and J. Davis, “Modifications to the Gooding Algorithm for Angles-Only Initial OrbitDetermination,” vol. 136, Jan. 2010.

[41] C. A. Miller and C. Frueh, “A COMPREHENSIVE COMPARISON AMONG CLASSICAL AND GOODING METHODS OF INITIAL ORBIT DETERMINATION IN OPTIMIZED ELECTRO- OPTICAL SENSOR NETWORKS,” May 2021.

[42] Y. Yin, Z. Li, C. Liu, Z. Kang, J. Sun, and L. Chen, “Improved Initial Orbit Determination Based on the Gooding Method of Low Earth Orbit Space Debris Using Space-Based Observations,” *Remote Sensing*, vol. 15, no. 21, Nov. 2023.

[43] W. Mitchell, “Gooding_IOD,” 2022. [Online]. Available: https://github.com/BillyMitchell97/Gooding_IOD

[44] GCC Wiki. (2026) Gfortran — the GNU Fortran compiler, part of GCC. [Online]. Available: https://gcc.gnu.org/wiki/GFortran

[45] L. Chen, C. Liu, Z. Li, and Z. Kang, “A New Triangulation Algorithm for Positioning Space Debris,” *Remote Sensing*, vol. 13, no. 23, p. 4878, Dec. 2021.

[46] H. Hwang, S.-Y. Park, and E. Lee, “Angles-Only Initial Orbit Determination of Low Earth Orbit (LEO) Satellites Using Real Observational Data,” *Journal of Astronomy and Space Sciences*, vol. 36, no. 3, pp. 187–197, Aug. 2019.

[47] F. Mart´inez, A. A. Maté, J. Fernández Sánchez, L. A. Garc´ia, and J. J. Grau, “Comparison of angles only initial orbit determination algorithms for space debris cataloguing,” *Journal of Aerospace Engineering, Sciences and Applications*, vol. 4, Jan. 2012.

[48] Ansys STK. (2026) Ephemeris File Format (*.e). [Online]. Available: https://help.agi.com/stk/#stk/importfiles-02.htm?Highlight=ephemeris

[49] University of Calgary. (2013, Sep.) CASSIOPE SPACECRAFT (Swarm-E) PROCESSED DATA HANDBOOK-Coordinate Systems. [Online]. Available: https://epop.phys.ucalgary.ca/data-handbook/coordinate-systems/